IPPP/10/31
DCPT/10/62
TUM–HEP–756/10

Theoretical and Phenomenological Constraints on Form Factors for Radiative and Semi-Leptonic B-Meson Decays

Aoife Bharucha[*,1], Thorsten Feldmann[†,2], Michael Wick[‡,2]

[1] *IPPP, Department of Physics, University of Durham, Durham DH1 3LE, UK*

[2] *Physik-Department, Technische Universität München, D-85748 Garching, Germany*

Abstract

We study transition form factors for radiative and rare semi-leptonic B-meson decays into light pseudoscalar or vector mesons, combining theoretical constraints and phenomenological information from Lattice QCD, light-cone sum rules, and dispersive bounds. We pay particular attention to form factor parameterisations which are based on the so-called series expansion, and study the related systematic uncertainties on a quantitative level. In this context, we also provide the NLO corrections to the correlation function between two flavour-changing tensor currents, which enters the unitarity constraints for the coefficients in the series expansion.

[*]a.k.m.bharucha@durham.ac.uk
[†]thorsten.feldmann@ph.tum.de
[‡]michael.wick@ph.tum.de

Contents

1 Introduction

At the upcoming LHC experiments (notably LHCb), exclusive B-meson decays will play one of the major roles for precision tests of the flavour sector in the Standard Model (SM) and its possible New Physics (NP) extensions [1, 2]. In order to extract information about the underlying short-distance flavour transitions, hadronic matrix elements will be required as theoretical input, and the precision to which they can be predicted will be essential for the success of the flavour program at LHCb. The most prominent example are transition form factors (FFs) for B-meson decays into light mesons, which will be the subject of this work. Being non-perturbative hadronic quantities, the theoretical calculation of FFs requires techniques such as Lattice QCD (see e.g. [3–7]) or QCD sum rules on the light cone (LCSR, see e.g. [8,9], and [10] and references therein). The two methods are complementary with respect to the momentum transfer q^2 between the initial and final-state mesons: In Lattice QCD, results are more easily obtainable at high values of q^2, as discretisation effects can only be controlled for small momenta of the final state in units of the Lattice spacing. This is in contrast to the LCSR method, which involves an expansion in inverse powers of the energy of the light daughter meson that is valid for low values of q^2.

Different FF parameterisations, which can be used to interpolate between the results for small and large momentum transfer, have been suggested in the literature; a good review can be found in [6]. These include simple pole-type parameterisations, like the Bećirević–Kaidalov (BK) approach [11], or variants like the Ball–Zwicky (BZ) parametrisation [8]. Another representation is found from the Omnes solution to the dispersion relation, see the discussion in [12, 13]. In this paper, we will make use of the so-called Series Expansion (SE), which was advocated in Refs. [14–18]. Here, one can make use of dispersive bounds to obtain additional theoretical constraints on the expansion coefficients. A simplified version of the SE (SSE) was recently suggested in [13]. The aim of this work is to use the SE/SSE to describe the transition FFs on the basis of recent Lattice and LCSR results, including a detailed analysis of systematic errors. We will focus in particular on the FFs entering $B \to V\gamma$, $B \to L\,\ell^+\ell^-$, $B \to L\nu\bar{\nu}$ decays, where $L = P, V$ is a light vector or pseudoscalar meson. We will give numerical results for $B \to \rho, K, K^*$ and $B_s \to \phi$ transitions, which are particularly interesting with respect to NP studies, see e.g. [1, 2, 19–23]. (Detailed phenomenological studies for FFs relevant for the determination of the CKM elements $|V_{ub}|$ and $|V_{cb}|$ from semi-leptonic B decays can be found in the recent literature [3–5, 13, 24].) For the discussion of dispersive bounds for tensor FFs, we will include the result of a precise calculation of the tensor current two-point correlator at NLO in the QCD coupling constant, including the leading non-perturbative corrections from quark and gluon condensates.

Our paper is organized as follows. In Section 2, we provide convenient definitions for the B-meson FFs and introduce the idea of the SE/SSE. In Section 3, we review the derivation of dispersive bounds from current-correlation functions and summarize the results for the profile functions obtained from the operator-product expansion. We apply our formalism to $B \to K$, $B \to \rho$, $B \to K^*$ and $B_s \to \phi$ FFs, by fitting the (truncated) SE/SSE to theoretical "data" from Lattice QCD and/or LCSRs in Section 4.3. Our conclusions are presented in Section 5, and some technical details are given in the Appendix.

2 Form Factors

In this section, we will first provide the definitions for the various B-meson FFs in question, fix the notation to be used in the subsequent discussion, and introduce the SE/SSE.

2.1 Definition of Form Factors and Helicity Amplitudes

The hadronic matrix elements for transitions between a pseudoscalar B meson and a generic (light) pseudoscalar meson are usually written in terms of three FFs $f_0(q^2)$, $f_+(q^2)$ and $f_T(q^2)$, which depend on the momentum transfer $q^2 = (p-k)^2$,

$$\begin{aligned}
\langle P(k)|\bar{q}\gamma_\mu b|B(p)\rangle &= \left(p_\mu + k_\mu - q_\mu \frac{m_B^2 - m_P^2}{q^2}\right) f_+(q^2) + \frac{m_B^2 - m_P^2}{q^2}\, q_\mu\, f_0(q^2)\,, \\
\langle P(k)|\bar{q}\sigma_{\mu\nu}q^\nu b|B(p)\rangle &= \frac{i}{m_B + m_P}\left(q^2(p+k)_\mu - (m_B^2 - m_P^2)\, q_\mu\right) f_T(q^2)\,. \qquad (1)
\end{aligned}$$

At zero momentum transfer, the additional relation $f_+(0) = f_0(0)$ holds.

Similarly, the matrix elements for the transition between a B-meson and a generic vector meson[1] can be written in terms of FFs $V(q^2)$, $A_{0-3}(q^2)$, $T_{1-3}(q^2)$, which are conventionally defined as

$$\begin{aligned}
\langle V(k,\varepsilon)|\bar{q}\gamma_\mu b|\bar{B}(p)\rangle &= i\epsilon_{\mu\nu\rho\sigma}\,\varepsilon^{*\nu}(k)\, p^\rho k^\sigma\, \frac{2V(q^2)}{m_B + m_V}\,, \\
\langle V(k,\varepsilon)|\bar{q}\gamma_\mu\gamma_5 b|\bar{B}(p)\rangle &= -\varepsilon^*_\mu(k)\,(m_B + m_V)\, A_1(q^2) + (p+k)_\mu\,(\varepsilon^*(k)\cdot q)\,\frac{A_2(q^2)}{m_B + m_V} \\
&\quad + q_\mu\,(\varepsilon^*(k)\cdot q)\,\frac{2m_V}{q^2}\left(A_3(q^2) - A_0(q^2)\right)\,, \qquad (2)
\end{aligned}$$

where $A_0(0) = A_3(0)$. For transitions involving a tensor current, the matrix elements are characterised by the tensor FFs,

$$\begin{aligned}
\langle V(k,\varepsilon)|\bar{q}\sigma_{\mu\nu}q^\nu b|\bar{B}(p)\rangle &= i\epsilon_{\mu\nu\rho\sigma}\,\varepsilon^{*\nu}\, p^\rho k^\sigma\, 2T_1(q^2)\,, \\
\langle V(k,\varepsilon)|\bar{q}\sigma_{\mu\nu}q^\nu\gamma_5 b|\bar{B}(p)\rangle &= T_2(q^2)\left(\varepsilon^*_\mu(k)\,(m_B^2 - m_V^2) - (\varepsilon^*(k)\cdot q)\,(p+k)_\mu\right) \\
&\quad + T_3(q^2)(\varepsilon^*(k)\cdot q)\left(q_\mu - \frac{q^2}{m_B^2 - m_V^2}\,(2p-q)_\mu\right)\,, \qquad (3)
\end{aligned}$$

where $T_1(0) = T_2(0)$. The equations of motion for the quarks imply the additional constraint

$$A_3(q^2) = \frac{m_B + m_V}{2m_V}\, A_1(q^2) - \frac{m_B - m_V}{2m_V}\, A_2(q^2)\,, \qquad (4)$$

and therefore the $B \to V$ transitions are characterized by seven independent FFs.

[1] Our phase convention for the vector state differs by a relative factor of i from the convention that is used, for instance, in [9].

The above constitute the standard definitions for the FFs widely used in the literature. However, for this work, we find it convenient to work with certain linear combinations of these, dubbed helicity amplitudes in Ref. [16]. This is primarily to diagonalize the unitarity relations, which shall be used to derive the dispersive bounds on certain FF parameterisations. The helicity amplitudes also have definite spin-parity quantum numbers, which is useful when considering the contribution of excited states. In addition, they have simple relations to the universal FFs, appearing in the heavy-quark and/or large-energy limit (see appendix B), and lead to simple expressions for the observables in $B \to L\,\ell^+\ell^-$ decays in the naive factorization approximation. To put the contributions to the various correlation functions entering the dispersive bounds on an equal footing, we also choose a particular normalization convention and define new $B \to P$ vector FFs via

$$\mathcal{A}_{V,\sigma}(q^2) = \sqrt{\frac{q^2}{\lambda}}\,\varepsilon_\sigma^{*\mu}(q)\,\langle P(k)|\bar{q}\,\gamma_\mu\,b|\bar{B}(p)\rangle\,. \tag{5}$$

Here

$$\lambda = \big((m_B - m_P)^2 - q^2\big)\,\big((m_B + m_P)^2 - q^2\big) \equiv (t_- - q^2)(t_+ - q^2) \tag{6}$$

is a standard kinematic function, and $\varepsilon_\sigma^{*\mu}(q)$ are transverse ($\sigma = \pm$), longitudinal ($\sigma = 0$) or time-like ($\sigma = t$) polarization vectors as defined in (60) in the appendix. This implies

$$\mathcal{A}_{V,0}(q^2) = f_+(q^2)\,, \qquad \mathcal{A}_{V,t}(q^2) = \frac{m_B^2 - m_P^2}{\sqrt{\lambda}}\,f_0(q^2)\,, \tag{7}$$

while the transverse projections vanish. Similarly, for the $B \to P$ tensor FF, we define

$$\mathcal{A}_{T,\sigma}(q^2) = (-i)\sqrt{\frac{1}{\lambda}}\,\varepsilon_\sigma^{*\mu}(q)\,\langle P(k)|\bar{q}\,\sigma_{\mu\nu}q^\nu\,b|\bar{B}(p)\rangle\,. \tag{8}$$

Here, the only non-zero FF is[2]

$$\mathcal{A}_{T,0}(q^2) = \frac{\sqrt{q^2}}{m_B + m_P}\,f_T(q^2)\,. \tag{9}$$

A similar analysis for the $B \to V$ vector and axial-vector FFs yields

$$\mathcal{B}_{V,\sigma}(q^2) = \sqrt{\frac{q^2}{\lambda}}\sum_{\varepsilon(k)}\varepsilon_\sigma^{*\mu}(q)\,\langle V(k,\varepsilon(k))|\bar{q}\,\gamma_\mu(1-\gamma^5)\,b|\bar{B}(p)\rangle \tag{10}$$

[2]The newly defined tensor FF $\mathcal{A}_{T,0}(q^2)$ vanishes as $\sqrt{q^2}$, which might look somewhat artificial at first glance. However, the tensor current does not contribute to physical processes at $q^2 = 0$ anyway.

with

$$\begin{aligned}
\mathcal{B}_{V,0}(q^2) &= \frac{(m_B+m_V)^2\,(m_B^2-m_V^2-q^2)\,A_1(q^2)-\lambda\,A_2(q^2)}{2m_V\sqrt{\lambda}\,(m_B+m_V)}\,,\\
\mathcal{B}_{V,t}(q^2) &= A_0(q^2)\,,\\
\mathcal{B}_{V,1}(q^2) &\equiv -\frac{\mathcal{B}_{V,-}-\mathcal{B}_{V,+}}{\sqrt{2}} = \frac{\sqrt{2\,q^2}}{m_B+m_V}\,V(q^2)\,,\\
\mathcal{B}_{V,2}(q^2) &\equiv -\frac{\mathcal{B}_{V,-}+\mathcal{B}_{V,+}}{\sqrt{2}} = \frac{\sqrt{2\,q^2}\,(m_B+m_V)}{\sqrt{\lambda}}\,A_1(q^2)\,.
\end{aligned} \tag{11}$$

Finally, the $B\to V$ matrix elements with tensor currents are projected on

$$\mathcal{B}_{T,\sigma}(q^2) = \sqrt{\frac{1}{\lambda}}\sum_{\varepsilon(k)}\varepsilon_\sigma^{*\mu}(q)\,\langle V(k,\varepsilon(k))|\bar{q}\,\sigma_{\mu\alpha}q^\alpha(1+\gamma^5)\,b|\bar{B}(p)\rangle \tag{12}$$

giving rise to the FFs

$$\begin{aligned}
\mathcal{B}_{T,0}(q^2) &= \frac{\sqrt{q^2}\,(m_B^2+3m_V^2-q^2)}{2m_V\sqrt{\lambda}}\,T_2(q^2) - \frac{\sqrt{q^2\,\lambda}}{2m_V\,(m_B^2-m_V^2)}\,T_3(q^2)\\
\mathcal{B}_{T,1}(q^2) &= -\frac{\mathcal{B}_{V,-}-\mathcal{B}_{V,+}}{\sqrt{2}} = \sqrt{2}\,T_1(q^2)\,,\\
\mathcal{B}_{T,2}(q^2) &= -\frac{\mathcal{B}_{V,-}+\mathcal{B}_{V,+}}{\sqrt{2}} = \frac{\sqrt{2}\,(m_B^2-m_V^2)}{\sqrt{\lambda}}\,T_2(q^2)\,.
\end{aligned} \tag{13}$$

2.2 Series Expansion

2.2.1 Resonances

An important factor in determining the shape of the FF is the presence of low-lying resonances with appropriate quantum numbers and mass $m_{\rm R}$ in the range $t_- < m_{\rm R}^2 < t_+$. Common to most parameterisations is the inclusion of the low-lying resonance by a simple pole. The various descriptions differ in the modelling of the continuous part. In the following, we use the abbreviation $P(q^2) = 1 - q^2/m_R^2$. If multiple resonances are present in the given region, then $P(q^2)$ should be a product of such poles, and if no resonances are present then $P(q^2) = 1$. A summary of the relevant resonance masses is provided in Table 1.

2.2.2 Series Expansion(SE)

The SE has its origin in dispersive relations [14–16,18]. The starting point is to extend the FFs defined in the physical range (from $q^2 = 0$ to $t_- = (m_B - m_L)^2$) to analytic functions throughout the complex $t = q^2$ plane, except for along the branch cut at the threshold for production of real BP/BV pairs at $q^2 \geq t_+ = (m_B + m_L)^2$. If low-lying resonances are

Table 1: Summary of the masses of low-lying B_d and B_s resonances, using PDG values [25] and/or theoretical estimates from heavy-quark/chiral symmetry [26]. Notice that the mass values for $(0^+, 1^+)$ predicted in [26] have not been confirmed experimentally, yet. Instead the PDG quotes "effective" resonances $B_J^*(5698)$ and $B_{sJ}^*(5853)$ with undetermined spin/parity.

Transition	J^P	Mass (GeV)	J^P	Mass (GeV)	Ref.
$b \to d$	0^-	5.28	1^-	5.33	[25]
	0^+	5.63	1^+	5.68	[26]
	1^+	5.72	2^+	5.75	[25]
$b \to s$	0^-	5.37	1^-	5.42	[25]
	0^+	5.72	1^+	5.77	[26]
	1^+	5.83	2^+	5.84	[25]

present below t_+, they are accounted for by the so called Blaschke factor $B(t)$, see below. Complex analysis can then be used to map the cut t–plane onto the unit disc in terms of the coordinate $z(t)$. The variable $z(t)$ is found to be an excellent expansion parameter for the FFs. Furthermore, with an appropriately chosen normalization function $\phi_f(t)$, one obtains simple dispersive bounds on the coefficients of the SE, see below. We will discuss the calculation of the functions $\phi_f(t)$ as well as the derivation of the dispersive bounds in greater detail in Section 3. The Series Expansion (SE) then corresponds to the following FF parametrisation,

$$f(t) = \frac{1}{B(t)\,\phi_f(t)} \sum_k \alpha_k\, z^k(t)\,, \tag{14}$$

with

$$z(t) \equiv z(t, t_0) = \frac{\sqrt{t_+ - t} - \sqrt{t_+ - t_0}}{\sqrt{t_+ - t} + \sqrt{t_+ - t_0}}\,. \tag{15}$$

Here $0 \le t_0 < t_-$ is a free parameter which can be optimised to reduce the maximum value of $|z(t)|$ in the physical FF range,

$$t_0\big|_{\rm opt.} = t_+ \left(1 - \sqrt{1 - \frac{t_-}{t_+}}\right)\,. \tag{16}$$

We will later see that with the optimised value for t_0, the FFs can be well described by a SE which is truncated after the second term proportional to $z(t)$. Other values of t_0 (e.g. $t_0 = 0$) are still allowed but sometimes require to go to higher order in the SE.

As a crucial property, the function $z(t)$ satisfies $|z(t)| \equiv 1$ in the pair-production region, $t \ge t_+$. The Blaschke factor is thus chosen as $B(t) = z(t, m_{\rm R}^2)$. As for $P(q^2)$ defined above, if multiple resonances are present, then $B(t)$ is a product of the corresponding Blaschke factors. Further discussion about the physical basis for the SE is found in Ref. [16].

2.2.3 Simplified Series Expansion (SSE)

Another form of the Series Expansion method can also be considered. Instead of the Blaschke factor $B(t)$, one can use a simple pole $P(q^2)$ to account for low-lying resonances. This idea was proposed in Ref. [13], yielding

$$f(t) \;=\; \frac{1}{P(t)} \sum_k \tilde{\alpha}_k \, z^k(t, t_0) \,. \tag{17}$$

It was found that the dispersive bounds can still be imposed on the coefficients $\tilde{\alpha}_k$ of the SSE. We will discuss this and other issues concerning the validity of the simplifications in the following section.

3 Dispersive Bounds

The FFs describe the process $B \to L$ with $L = P, V$ in the decay region $0 < q^2 < t_- = (m_B - m_L)^2$. Using crossing symmetry, they can also describe the process in the pair-production region $q^2 > (m_B + m_L)^2$. This can be exploited to obtain a bound on parameters describing the FFs. A detailed derivation of this bound can be found in Refs. [15,17]. Here we provide a brief outline of the argument, in order to introduce our notation and to extend the method to tensor FFs.

The crucial observation of the idea of dispersive bounds (as it is for QCD sum rules) is the possibility to evaluate the correlator of two flavour-changing currents,

$$\Pi^X_{\mu\nu}(q^2) = i \int d^4x \, e^{i\,q\cdot x} \, \langle 0 | \, \mathrm{T} \, j^X_\mu(x) \, j^{\dagger\,X}_\nu(0) \, | 0 \rangle \;, \tag{18}$$

either by an operator product expansion (OPE) or by unitarity considerations. Here the relevant currents j^X_μ are defined as[3]

$$\begin{aligned} j^V_\mu &= \bar{q}\gamma_\mu b \,, & j^{V-A}_\mu &= \bar{q}\gamma_\mu(1-\gamma^5)b \,, \\ j^T_\mu &= \bar{q}\sigma_{\mu\alpha}q^\alpha b \,, & j^{T+A_T}_\mu &= \bar{q}\sigma_{\mu\alpha}q^\alpha(1+\gamma^5)b \,. \end{aligned} \tag{19}$$

Furthermore, we introduce longitudinal and transverse helicity projectors,

$$P^{\mu\nu}_L(q^2) = \frac{q^\mu q^\nu}{q^2} \,, \qquad P^{\mu\nu}_T(q^2) = \frac{1}{D-1}\left(\frac{q^\mu q^\nu}{q^2} - g^{\mu\nu}\right) \,, \tag{20}$$

which allow us to rewrite the correlation functions in terms of Lorentz scalars,

$$\Pi^X_I(q^2) \equiv P^{\mu\nu}_I(q^2) \, \Pi^X_{\mu\nu}(q^2) \,, \qquad (I = L, T). \tag{21}$$

[3] In phenomenological applications, we are only interested in the currents $j^{T+A_T}_\mu$. The connection to correlators with genuine tensor currents $j_{\mu\nu} = \bar{q}\sigma_{\mu\nu}q$ is given in Appendix D.

As $\Pi_I^X(q^2)$ is an analytic function, it satisfies the subtracted dispersion relation,

$$\chi_I^X(n) = \frac{1}{n!}\left.\frac{d^n\Pi_X(q^2)}{dq^{2^n}}\right|_{q^2=0} = \frac{1}{\pi}\int_0^\infty dt\left.\frac{\mathrm{Im}\,\Pi_I^X(t)}{(t-q^2)^{n+1}}\right|_{q^2=0}, \tag{22}$$

where the number of subtractions n is chosen to render the resulting function $\chi_I^X(n)$ finite.

3.1 Hadronic representation of the Correlator

Unitarity allows us to express $\mathrm{Im}\,\Pi_I^X(q^2)$ as the positive definite sum over all hadronic states Γ with allowed quantum numbers:

$$\mathrm{Im}\,\Pi_I^X(q^2) = \frac{1}{2}\sum_\Gamma\int d\rho_\Gamma\,(2\pi)^4\,\delta^4(q-p_\Gamma)\,P_I^{\mu\nu}\;\langle 0|\,j_\mu^X\,|\Gamma\rangle\,\langle\Gamma|\,j_\nu^{\dagger X}\,|0\rangle\;. \tag{23}$$

where p_Γ is the total momentum of the final state, and $d\rho_\Gamma$ contains the appropriate phase-space weighting. For a particular choice of intermediate state, $\Gamma = BL$, we define

$$\mathrm{Im}\,\Pi_{I,BL}^X(q^2) = \eta\int d\rho_{BL}\,P_I^{\mu\nu}\;\langle 0|\,j_\mu^X\,|BL\rangle\,\langle BL|\,j_\nu^{\dagger X}\,|0\rangle\;, \tag{24}$$

where η is an isospin-degeneracy factor for a given channel, and we relegate the contribution from phase space to the function

$$d\rho_{BL} = \frac{1}{4\pi^2}\int\frac{d^3p_B}{2E_B}\,\frac{d^3p_L}{2E_L}\,\delta^4(q-p_B-p_L)\,. \tag{25}$$

Clearly, this results in the inequality

$$\mathrm{Im}\Pi_{I,BL}^X(t) \le \mathrm{Im}\Pi_I^X(t)\,. \tag{26}$$

Now, by extending the FFs to analytic functions throughout the t–plane, except for along the branch cut at the threshold for production of real BL pairs, one can use crossing symmetry to relate the matrix elements $\langle 0|\,j^X\,|BL\rangle$ to $\langle B|\,j^X\,|L\rangle$. The latter can be rewritten in terms of FFs, as defined in Section 2. As stated earlier, we use helicity-based linear combinations of the traditional FFs, such that all production amplitudes 'diagonalize':

$$\begin{aligned}
P_T^{\mu\nu}\,\langle P|j_\mu^V|B\rangle\langle B|j_\nu^{\dagger V}|P\rangle &= \frac{\lambda}{3q^2}\,|\mathcal{A}_{V,0}|^2\;,\\
P_L^{\mu\nu}\,\langle P|j_\mu^V|B\rangle\langle B|j_\nu^{\dagger V}|P\rangle &= \frac{\lambda}{q^2}\,|\mathcal{A}_{V,t}|^2\;,\\
P_T^{\mu\nu}\,\langle P|j_\mu^T|B\rangle\langle B|j_\nu^{\dagger T}|P\rangle &= \frac{\lambda}{3}\,|\mathcal{A}_{T,0}|^2\;,
\end{aligned} \tag{27}$$

for B decays into pseudoscalars, and

$$\begin{aligned} P_T^{\mu\nu}\,\langle V|j_\mu^{V-A}|B\rangle\langle B|j_\nu^{\dagger,V-A}|V\rangle &= \frac{\lambda}{3q^2}\sum_{i=0}^{2}|\mathcal{B}_{V,i}|^2\,, \\ P_L^{\mu\nu}\,\langle V|j_\mu^{V-A}|B\rangle\langle B|j_\nu^{\dagger,V-A}|V\rangle &= \frac{\lambda}{q^2}\,|\mathcal{B}_{V,t}|^2\,, \\ P_T^{\mu\nu}\,\langle V|j_\mu^{T+A_T}b|B\rangle\langle B|j_\nu^{\dagger,T+A_T}b|V\rangle &= \frac{\lambda}{3}\sum_{i=0}^{2}|\mathcal{B}_{T,i}|^2\,. \end{aligned} \tag{28}$$

We can now express $\mathrm{Im}\,\Pi^X_{I,BL}$ in compact form,

$$\mathrm{Im}\,\Pi^X_{I,BL} = \eta\int d\rho_{BL}\,\frac{\lambda}{3t}\left|A_I^X\right|^2 = \frac{\eta}{48\pi}\,\frac{\lambda^{3/2}}{t^2}\left|A_I^X\right|^2\,, \tag{29}$$

where the $\left|A_I^X\right|^2$ can be read off (27,28),

$$\left|A_T^V\right|^2 = |\mathcal{A}_{V,0}|^2\,,\qquad \left|A_L^V\right|^2 = 3\,|\mathcal{A}_{V,t}|^2\,,\qquad \left|A_T^T\right|^2 = q^2\,|\mathcal{A}_{T,0}|^2\,, \tag{30}$$

for decays into pseudoscalars, and

$$\left|A_T^{V-A}\right|^2 = \sum_{i=0}^{2}|\mathcal{B}_{V,i}|^2\,,\qquad \left|A_L^{V-A}\right|^2 = 3\,|\mathcal{B}_{V,t}|^2\,,\qquad \left|A_T^{T+A_T}\right|^2 = q^2\sum_{i=0}^{2}|\mathcal{B}_{T,i}|^2\,, \tag{31}$$

for decays into vector mesons.

3.2 OPE for the Correlator

Alternatively, we can examine the correlator (18), using an OPE for the T-ordered product of currents in the limit $q^2 = 0 \ll t_+$. The standard expansion takes the form [27–29]

$$i\int dx\,e^{i\,q\cdot x}\,P_I^{\mu\nu}\,\mathrm{T}\left\{j_\mu^X(x)\,j_\nu^{\dagger\,X}(0)\right\} = \sum_{k=1}^{\infty}C_{I,k}^X(q)\,\mathcal{O}_k\,, \tag{32}$$

where $C^X_{I,n}(q)$ are Wilson coefficients for a given current X and projector I, and $\mathcal{O}_n$ are local gauge-invariant operators, consisting of quark and gluon fields. Here, the operators are ordered by increasing dimension k. We can use the above, to express the correlator,

$$\Pi^X_{I,\mathrm{OPE}}(q^2) = \sum_{k=1}^{\infty}C_{I,k}^X(q^2)\,\langle O_k\rangle\,. \tag{33}$$

Besides the identity operator, whose Wilson coefficient contains the purely perturbative contribution to the correlator, we will specifically consider the first few operators related to the non-perturbative contribution from the quark condensate $\langle m_q\,\bar{q}q\rangle$, the gluon condensate $\langle\frac{\alpha_s}{\pi}\,G^2\rangle$, and the mixed condensate $\langle g_s\,\bar{q}\,(\sigma\cdot G)\,q\rangle$. We will elaborate on our calculation of the Wilson coefficients, $C^X_{I,k}(q^2)$, later. Specifically, we must calculate the Wilson coefficients entering the functions $\chi_I^X(n)$ in (22).

3.3 Bounds on coefficients in the SE

Using (26), we find

$$\frac{1}{\pi}\int\limits_0^\infty dt\,\frac{\text{Im}\,\Pi^X_{I,BL}(t)}{(t-q^2)^{n+1}}\bigg|_{q^2=0}=\frac{1}{\pi}\int\limits_{t_+}^\infty dt\,\frac{\eta\,\lambda^{3/2}(t)}{48\pi\,t^{n+3}}\left|A_I^X(t)\right|^2\le\chi_I^X(n)\,, \tag{34}$$

where $\chi_I^X\equiv\chi_{I,\text{OPE}}^X$ is calculated from (33). Mapping the pair-production region $t\ge t_+$ onto the unit circle $|z(t)|=1$, this inequality could be written in the form

$$\frac{1}{2\pi i}\oint\frac{dz}{z}\,|\phi_I^X\,A_I^X|^2(z)\le 1\quad\Leftrightarrow\quad\frac{1}{\pi}\int_{t_+}^\infty\frac{dt}{t-t_0}\sqrt{\frac{t_+-t_0}{t-t_+}}\,|\phi_I^X\,A_I^X|^2(t)\le 1\,, \tag{35}$$

where the function $|\phi_I^X(t)|^2$ can be obtained by comparing (35) and (34), and using $\lambda(t)=(t_+-t)(t_--t)$,

$$|\phi_I^X(t)|^2=\frac{\eta}{48\pi\,\chi_I^X(n)}\,\frac{(t-t_+)^2}{(t_+-t_0)^{1/2}}\,\frac{(t-t_-)^{3/2}}{t^{n+2}}\,\frac{t-t_0}{t}\,. \tag{36}$$

The isospin-degeneracy factor η takes the values 3/2, 2 and 1 for $B\to\rho$, $B\to K^{(*)}$ and $B_s\to\phi$ respectively. We may now generically write the helicity-based FFs $A_I^X(t)$ as

$$A_I^X(t)=\frac{(\sqrt{-z(t,0)})^m(\sqrt{z(t,t_-)})^l}{B(t)\,\phi_I^X(t)}\,\sum_{k=0}^\infty\alpha_k\,z^k \tag{37}$$

with real coefficients α_k, and a Blaschke factor $B(t)=\prod_i z(t,m_{R_i}^2)$, representing poles due to sub-threshold resonances of masses m_{R_i}, and satisfying $|B(t)|=1$ in the pair-production region. The additional factors $(\sqrt{-z(t,0)})^m$ and $(\sqrt{z(t,t_-)})^l$ have been added to take into account the unconventional normalisation of our FF functions through factors of $\sqrt{q^2}$ and $\sqrt{\lambda}$ (e.g. $m=1$ for $\mathcal{A}_{T,0}$, and $l=-1$ for $\mathcal{A}_{V,t}$, cf. above).[4] The function $\phi_I^X(t)$ has to be constructed in such a way that its absolute value satisfies Eq. (36), while (37) retains the analytical properties of the FF. This can easily be achieved by replacing potential poles and cuts in $\sqrt{|\phi_I^X(t)|^2}$, by making replacements of the form

$$\frac{1}{t-X}\to\frac{-z(t,X)}{t-X}\,, \tag{38}$$

which is allowed as $|z(t,X)|=1$ in the pair-production region. This results in (see also [30])

$$\phi_I^X(t)=\sqrt{\frac{\eta}{48\pi\chi_I^X(n)}}\,\frac{(t-t_+)}{(t_+-t_0)^{1/4}}\left(\frac{z(t,0)}{-t}\right)^{(3+n)/2}\left(\frac{z(t,t_0)}{t_0-t}\right)^{-1/2}\left(\frac{z(t,t_-)}{t_--t}\right)^{-3/4}\,. \tag{39}$$

[4]These factors could also be considered as part of the Blaschke factor. Note that under a change of normalisation convention for the FFs, both, the so-constructed Blaschke factor as well as the function $\phi(t)$ have to be modified, while the coefficients α_k of the SE remain the same.

Inserting the parametrisation (37) into (35), and using $|z(t,t_0)| = |z(t,m_R^2)| = |z(t,0)| = 1$, the integration $dz/z = d\varphi$ along the unit circle is trivial, yielding the desired bound on the coefficients α_k,

$$\sum_{k=0}^{\infty} \alpha_k^2 < 1\,. \tag{40}$$

For decays into vector mesons, using an analogous parametrisation as (37) for each *individual* FF contribution in (31), one obtains a bound on the sum of the corresponding coefficients. As an example, let us consider $A_T^{V-A}(t)$, where we parameterise

$$\begin{aligned}
\mathcal{B}_{V,0}(t) &= \frac{1}{B(t)\,\sqrt{z(t,t_-)}\,\phi_T^{V-A}(t)} \sum_{k=0}^{K-1} \beta_k^{(V,0)}\, z^k\,, \\
\mathcal{B}_{V,1}(t) &= \frac{\sqrt{-z(t,0)}}{B(t)\,\phi_T^{V-A}(t)} \sum_{k=0}^{K-1} \beta_k^{(V,1)}\, z^k\,, \\
\mathcal{B}_{V,2}(t) &= \frac{\sqrt{-z(t,0)}}{B(t)\,\sqrt{z(t,t_-)}\,\phi_T^{V-A}(t)} \sum_{k=0}^{K-1} \beta_k^{(V,2)}\, z^k\,,
\end{aligned} \tag{41}$$

resulting in the dispersive bound

$$\sum_{k=0}^{K-1} \Big((\beta_k^{(V,0)})^2 + (\beta_k^{(V,1)})^2 + (\beta_k^{(V,2)})^2 \Big) < 1\,. \tag{42}$$

3.4 The coefficients $\chi_I^X(n)$

In Table 2 we summarize the numerical result of our calculation of the various coefficients $\chi_I^X(n)$, which enter the functions $\phi_I^X(t)$ in the SE. We quote individual numbers for the perturbative LO and NLO results, as well as from the condensate contributions, for two different values of light-quark masses, $m_q = m_d$ and $m_q = m_s$. Also the number of subtractions is indicated. Details of the calculation as well as analytical formulas can be found in Appendix C. As can be observed from Table 2, the NLO perturbative corrections are essential for a reliable estimate for the coefficients $\chi_I^X(n)$, while the quark condensate gives only small contributions, and the gluon condensate and the mixed quark-gluon condensate are negligible.

4 Form Factor Fits to Theoretical Data

4.1 Theory Input from Lattice and LCSR

There are two main methods to obtain theoretical predictions on B-meson decay FFs: Light-cone sum rules (LCSRs) and Lattice QCD. As mentioned in the introduction, these

Table 2: Summary of OPE results for the coefficients $\chi_I^X(n)$. The following parameter values have been used [27, 31–33]: $\mu = m_b = 4.2$ GeV, $m_d = 4.8$ MeV, $m_s = 104$ MeV, $\alpha_s = 0.2185$, $\langle \bar{d}d \rangle = (278 \text{ MeV})^3$, $\langle \bar{s}s \rangle = 0.8 \langle \bar{d}d \rangle$, $\left\langle \frac{\alpha_s}{\pi} G^2 \right\rangle = 0.038 \text{ GeV}^4$, $\langle \bar{q}Gq \rangle = (1.4 \text{ GeV})^2 \langle \bar{\text{q}}\text{q} \rangle$.

q	Correlator	Subtractions	LO	NLO	$\langle \bar{q}q \rangle$	$\left\langle \frac{\alpha}{\pi} G^2 \right\rangle$	$\langle \bar{q}Gq \rangle$	Σ
d	$100 \times m_b^2 \chi^S$	2	1.265	0.589	0.029	0.001	−0.003	1.88
	$100 \times m_b^2 \chi^P$	2	1.268	0.590	0.029	0.001	−0.003	1.88
	$100 \times \chi_L^V$	1	1.262	0.211	0.029	0.001	−0.003	1.50
	$100 \times \chi_L^A$	1	1.271	0.205	0.029	0.001	−0.003	1.50
	$100 \times m_b^2 \chi_T^V$	2	0.951	0.236	−0.029	−0.001	0.007	1.16
	$100 \times m_b^2 \chi_T^A$	2	0.948	0.237	−0.029	−0.001	0.007	1.16
	$100 \times m_b^2 \chi_T^T$	3	2.539	0.579	−0.029	−0.000	0.008	3.10
	$100 \times m_b^2 \chi_T^{AT}$	3	2.527	0.586	−0.029	−0.001	0.008	3.09
s	$100 \times m_b^2 \chi^S$	2	1.233	0.571	0.024	0.001	−0.003	1.83
	$100 \times m_b^2 \chi^P$	2	1.296	0.608	0.022	0.001	−0.003	1.93
	$100 \times \chi_L^V$	1	1.172	0.229	0.023	0.000	−0.003	1.42
	$100 \times \chi_L^A$	1	1.361	0.187	0.023	0.002	−0.003	1.57
	$100 \times m_b^2 \chi_T^V$	2	0.980	0.237	−0.022	0.000	0.005	1.20
	$100 \times m_b^2 \chi_T^A$	2	0.916	0.238	−0.024	−0.002	0.006	1.13
	$100 \times m_b^2 \chi_T^T$	3	2.652	0.569	−0.023	0.001	0.006	3.21
	$100 \times m_b^2 \chi_T^{AT}$	3	2.404	0.603	−0.024	−0.002	0.007	2.99

techniques are largely complementary, as they perform best in different regimes of momentum transfer q^2. It is worth mentioning that certain decays, e.g. decays to unstable hadrons, are more challenging in Lattice QCD, and in some cases only quenched results exist for a subset of the FFs. On the other hand, LCSRs provide results for all decay channels considered in this work, including the complete set of seven FFs for $B \to K^*$ and $B_s \to \phi$, which so far have not been fully addressed by Lattice QCD. However, as LCSR results are only valid in the low–q^2 regime, in these cases further theoretical information is needed to extrapolate to large values of q^2, as will be discussed in the following subsections.

In our analysis, we will use the LCSR predictions from Refs. [8] and [9], taking 3(4) points at low values of q^2 as input, see Table 3. The quoted errors are extrapolated from the value quoted for $q^2 = 0$ in the references specified in the Table. Lattice data is available for $B \to \rho$ and $B \to K$ decays, and is as shown in Table 4.[5] For those data points which have an asymmetric statistical or systematic error, in order to perform the fit, we take the FF to be the central value in this statistical or systematic range, and take half the range to be the statistical or systematic error [34].

For $B \to \rho$ and $B \to K$ decays, we use LCSR and Lattice data to interpolate between the low and high–q^2 region. The result can be compared to the case where we extrapolate to the high–q^2 region only on the basis of LCSR predictions. This procedure will gives us an idea about the confidence in the extrapolations for those cases where Lattice data is lacking.

4.2 Parameterisation of FFs as Series Expansion

For those channels where where Lattice data is not available, it is essential to employ a FF parameterisation that takes into account the characteristic features of the FF shape as determined from the analyticity and unitarity consideration above. For every considered FF, we will therefore define a parameterisation based on the SE,

$$\begin{aligned}
\mathcal{A}_{V,0}(t) &= \frac{1}{B(t)\,\phi_T^V(t)} \sum_{k=0}^{K-1} \alpha_k^{(V,0)}\, z^k\,, \\
\mathcal{A}_{V,t}(t) &= \frac{1}{B(t)\,\sqrt{z(t,t_-)}\,\phi_L^V(t)} \sum_{k=0}^{K-1} \alpha_k^{(V,t)}\, z^k\,, \\
\mathcal{A}_{T,0}(t) &= \frac{\sqrt{-z(t,0)}}{B(t)\,\phi_T^T(t)} \sum_{k=0}^{K-1} \alpha_k^{(T,0)}\, z^k\,,
\end{aligned} \tag{43}$$

[5] We are very grateful to Sara Collins of the QCDSF collaboration for providing us with specific values for $B \to K$.

Table 3: Overview of LCSR points used, transformed to the helicity amplitude basis.

Decay	FF	LCSR/q^2 (GeV^2)				Ref.
$B \to K$	q^2	3	6	9	12	Table 3, [8]
	$\mathcal{A}_{V,0}$	0.40 ± 0.05	0.48 ± 0.06	0.59 ± 0.07	-	
	$\mathcal{A}_{V,t}$	0.40 ± 0.05	0.51 ± 0.06	0.65 ± 0.08	-	
	$\mathcal{A}_{T,0}$	0.13 ± 0.01	0.22 ± 0.02	0.34 ± 0.03	-	
$B \to \rho$	q^2	3	6	9	12	Table 8, [9]
	$\mathcal{B}_{V,0}$	0.37 ± 0.12	0.46 ± 0.13	0.60 ± 0.14	-	
	$\mathcal{B}_{V,1}$	0.16 ± 0.01	0.27 ± 0.02	0.41 ± 0.04	-	
	$\mathcal{B}_{V,2}$	0.16 ± 0.02	0.29 ± 0.03	0.46 ± 0.04	-	
	$\mathcal{B}_{V,t}$	0.37 ± 0.04	0.46 ± 0.04	0.58 ± 0.06	-	
	$\mathcal{B}_{T,0}$	0.17 ± 0.35	0.3 ± 0.26	0.47 ± 0.23	0.71 ± 0.22	
	$\mathcal{B}_{T,1}$	0.45 ± 0.04	0.55 ± 0.05	0.69 ± 0.06	0.9 ± 0.08	
	$\mathcal{B}_{T,2}$	0.46 ± 0.04	0.58 ± 0.05	0.76 ± 0.07	1.0 ± 0.1	
$B \to K^*$	q^2	3	6	9	12	Table 8, [9]
	$\mathcal{B}_{V,0}$	0.45 ± 0.13	0.56 ± 0.13	0.73 ± 0.15	-	
	$\mathcal{B}_{V,1}$	0.19 ± 0.02	0.32 ± 0.03	0.49 ± 0.04	-	
	$\mathcal{B}_{V,2}$	0.20 ± 0.02	0.35 ± 0.03	0.57 ± 0.06	-	
	$\mathcal{B}_{V,t}$	0.44 ± 0.04	0.54 ± 0.05	0.67 ± 0.06	-	
	$\mathcal{B}_{T,0}$	0.23 ± 0.36	0.39 ± 0.27	0.60 ± 0.24	0.90 ± 0.22	
	$\mathcal{B}_{T,1}$	0.59 ± 0.06	0.72 ± 0.07	0.89 ± 0.08	1.2 ± 0.1	
	$\mathcal{B}_{T,2}$	0.61 ± 0.06	0.77 ± 0.07	1.0 ± 0.1	1.4 ± 0.1	
$B_s \to \phi$	q^2	3	6	9	12	Table 8, [9]
	$\mathcal{B}_{V,0}$	0.55 ± 0.12	0.68 ± 0.13	0.85 ± 0.14	-	
	$\mathcal{B}_{V,1}$	0.2 ± 0.02	0.34 ± 0.03	0.52 ± 0.04	-	
	$\mathcal{B}_{V,2}$	0.21 ± 0.02	0.38 ± 0.04	0.62 ± 0.06	-	
	$\mathcal{B}_{V,t}$	0.56 ± 0.04	0.68 ± 0.05	0.85 ± 0.06	-	
	$\mathcal{B}_{T,0}$	0.26 ± 0.39	0.44 ± 0.29	0.67 ± 0.26	1.0 ± 0.3	
	$\mathcal{B}_{T,1}$	0.59 ± 0.06	0.72 ± 0.07	0.89 ± 0.08	1.2 ± 0.1	
	$\mathcal{B}_{T,2}$	0.61 ± 0.06	0.77 ± 0.07	1.0 ± 0.1	1.4 ± 0.1	

Table 4: Overview of Lattice points used, transformed to the helicity amplitude basis. Note that specific values for $B \to \rho$ are as in Table 2 of Ref. [12].

Decay	q^2 (GeV^2)	FF			Ref.
$B \to K$		$\mathcal{A}_{V,0}$	$\mathcal{A}_{V,t}$	$\mathcal{A}_{T,0}$	QCDSF [4]
	14.5	0.94 ± 0.19	1.1 ± 0.2	-	
	15.6	1.1 ± 0.2	1.3 ± 0.3	-	
	16.7	1.2 ± 0.2	1.5 ± 0.3	-	
	17.9	1.4 ± 0.3	1.8 ± 0.3	-	
	19.	1.6 ± 0.3	2.3 ± 0.4	-	
	20.1	1.9 ± 0.4	$3. \pm 0.6$	-	
	21.3	2.3 ± 0.4	4.4 ± 0.8	-	
	22.4	2.9 ± 0.6	8.7 ± 1.7	-	
$B \to \rho$		$\mathcal{B}_{V,0}$	$\mathcal{B}_{V,1}$	$\mathcal{B}_{T,2}$	UKQCD [7]
	12.7	0.64 ± 0.78	0.34 ± 0.27	0.9 ± 0.18	
	13.	0.71 ± 0.72	0.39 ± 0.25	0.96 ± 0.18	
	13.5	0.8 ± 0.66	0.48 ± 0.22	1.1 ± 0.2	
	14.	0.9 ± 0.62	0.58 ± 0.19	1.2 ± 0.2	
	14.5	1.0 ± 0.6	0.68 ± 0.16	1.3 ± 0.2	
	15.	1.1 ± 0.6	0.78 ± 0.15	1.4 ± 0.2	
	15.5	1.3 ± 0.7	0.89 ± 0.15	1.6 ± 0.2	
	16.	1.4 ± 0.8	1.0 ± 0.2	1.8 ± 0.2	
	16.5	1.6 ± 0.9	1.2 ± 0.3	2.1 ± 0.2	
	17.1	1.8 ± 1.2	1.4 ± 0.4	2.4 ± 0.2	
	17.6	2.1 ± 1.5	1.7 ± 0.6	2.7 ± 0.3	
	18.2	$2.5 \pm 2.$	2.1 ± 0.9	3.3 ± 0.3	

and

$$\begin{aligned}
\mathcal{B}_{V,t}(t) &= \frac{1}{B(t)\,\phi_L^{V-A}(t)} \sum_{k=0}^{K-1} \beta_k^{(V,t)}\, z^k\,, \\
\mathcal{B}_{T,0}(t) &= \frac{\sqrt{-z(t,0)}}{B(t)\,\sqrt{z(t,t_-)}\,\phi_T^{T+A_T}(t)} \sum_{k=0}^{K-1} \beta_k^{(T,0)}\, z^k\,, \\
\mathcal{B}_{T,1}(t) &= \frac{1}{B(t)\,\phi_T^{T+A_T}(t)} \sum_{k=0}^{K-1} \beta_k^{(T,1)}\, z^k\,, \\
\mathcal{B}_{T,2}(t) &= \frac{1}{B(t)\,\sqrt{z(t,t_-)}\,\phi_T^{T+A_T}(t)} \sum_{k=0}^{K-1} \beta_k^{(T,2)}\, z^k\,,
\end{aligned} \tag{44}$$

and $\mathcal{B}_{V,0-2}$ already given in (41). Here we have used our FF convention defined in (5,8,10,12) and explicitly quoted the pre-factors, necessary to obtain the correct analytical behaviour of our FFs.[6] In our fits below, we will find that in general the SE can be truncated after the first two terms, i.e. the parameter K can be set to 2. We should point out, however, that this does not necessarily imply that higher-order terms in the SE are negligible: Although $|z|^2 \ll 1$ in the semi-leptonic region, one may still have $|\alpha_2\, z^2| \sim |\alpha_1 z|$ if the coefficients satisfy $\alpha_1 \ll \alpha_2 \lesssim 1$. From the theoretical point of view, this reflects an irreducible source of uncertainty, which we will discuss in some detail for some specific examples in Sec. 4.4. From the practical point of view, we consider the truncated SE as a reasonable parameterisation which is easy to implement (and easy to refine) in phenomenological studies.

For simplicity, we will not explicitly implement the theoretical relations (64,65), that some of the FFs fulfil at $q^2 = 0$, into the fit, because they are automatically satisfied by the rather precise input from LCSR at this point. However, the helicity-based FF definition further implies a relation between the FFs $\mathcal{B}_{V,0}$ and $\mathcal{B}_{V,2}$, and similarly between $\mathcal{B}_{T,0}$ and $\mathcal{B}_{T,2}$, see (66) in the appendix, which we will implement as an additional constraints on the corresponding coefficients in the SE. From the above parameterisations, the SSE is obtained by the replacements

$$\phi_I^X(t) \to 1\,, \quad B(t) \to P(t)\,, \quad \sqrt{-z(t,0)} \to \sqrt{q^2}/m_B\,, \quad \sqrt{z(t,t_-)} \to \sqrt{\lambda}/m_B^2\,, \tag{45}$$

with new coefficients $\tilde{\alpha}_k$ and $\tilde{\beta}_k$.

[6] In Refs. [18] and [13, 17], the predictions from perturbative QCD for the scaling of the FFs at large values of q^2 have been used as an additional constraint on the shape of the FFs. We have found that these constraints do not influence the FF fits in the decay region significantly. As the asymptotic behaviour of exclusive observables in QCD is still a matter of controversy, we therefore find it safer and simpler not to include these constraints in our parameterisation.

4.2.1 Unitarity constraints

For the SE parameterisation, the unitarity constraints take the form

$$\sum_{k=0}^{K-1} (\alpha_k)^2 \leq 1 \quad \text{for } \mathcal{A}_{V,0} \text{ and } \mathcal{A}_{T,0}, \qquad 3\sum_{k=0}^{K-1} (\alpha_k)^2 \leq 1 \quad \text{for } \mathcal{A}_{V,t}, \tag{46}$$

and

$$\begin{aligned}
&3\sum_{k=0}^{K-1} (\beta_k^{(V,t)})^2 \leq 1 \quad \text{for } \mathcal{B}_{V,t}, \\
&\sum_{k=0}^{K-1} \left\{ (\beta_k^{(V,0)})^2 + (\beta_k^{(V,1)})^2 + (\beta_k^{(V,2)})^2 \right\} \leq 1 \quad \text{for } \mathcal{B}_{V,0}, \mathcal{B}_{V,1}, \text{ and } \mathcal{B}_{V,2}, \\
&\sum_{k=0}^{K-1} \left\{ (\beta_k^{(T,0)})^2 + (\beta_k^{(T,1)})^2 + (\beta_k^{(T,2)})^2 \right\} \leq 1 \quad \text{for } \mathcal{B}_{T,0}, \mathcal{B}_{T,1}, \text{ and } \mathcal{B}_{T,2}.
\end{aligned} \tag{47}$$

For the SSE parameterisation, imposing the unitarity bound is more complicated, as shown in Ref. [13]. We repeat the derivation of this bound in order to define notation used later. One first compares the SE and SSE parameterisations:

$$\sum_{k=0}^{K-1} \alpha_k \, z^k = \Lambda(z) \sum_{k=0}^{K-1} \tilde{\alpha}_k \, z^k \tag{48}$$

One can simply obtain $\Lambda(z)$ by combining the prefactors from the SE expansion with the prefactors from the SSE expansion, and expressing the result as a function of $z(t, t_0)$. Since z is a small parameter, we can expand $\Lambda(z)$ in powers of z:

$$\Lambda(z) = \sum_k \zeta_k \, z^k. \tag{49}$$

We can therefore obtain a relation between the coefficients α_k and $\tilde{\alpha}_k$,

$$\alpha_i = \sum_{k=0}^{\min[K-1,i]} \zeta_{i-k} \, \tilde{\alpha}_k \,, \qquad 0 \leq i \leq K-1 \,, \tag{50}$$

which results in bounds of the type

$$\sum_{j,k=0}^{K-1} C_{jk} \, \tilde{\alpha}_j \, \tilde{\alpha}_k \leq 1 \,, \tag{51}$$

where

$$C_{jk} = \sum_{i=0}^{K-1-\max[j,k]} \zeta_i \, \zeta_{i+|j-k|} \tag{52}$$

is a positive definite matrix.

4.3 Fitting prescription

We perform a fit to the LCSR data, as well as, where possible, a combined fit to the LCSR and Lattice data, by minimising a χ^2 function defined by

$$\chi^2(\vec{\theta}) = \Big(F_i - F(t_i, \vec{\theta})\Big) \left[V^{-1}\right]_{ij} \Big(F_j - F(t_j, \vec{\theta})\Big) \,, \tag{53}$$

where $\vec{\theta}$ contains the parameters of a given FF parameterisation, F_i are the FF values from LCSR/Lattice at given points t_i, and V_{ij} are elements of the covariance matrix as defined below.

As explained above, we are going to investigate parameterisations based on two variants of the SE, where the parameters will be subject to additional constraints derived from dispersive bounds on the FFs.

- In the conventional series expansion (SE), we use (14), and truncate the series after the first 2 terms, such that

$$\vec{\theta} = \{\alpha_0, \alpha_1\} \,, \qquad \sum \alpha_i^2 \overset{!}{<} 1 \,.$$

- The simplified series expansion (SSE) uses (17), with

$$\vec{\theta} = \{\tilde{\alpha}_0, \tilde{\alpha}_1\} \,, \qquad \sum_{i,j=0}^{1} C_{ij}\, \tilde{\alpha}_i \tilde{\alpha}_j \overset{!}{<} 1 \,,$$

  where the matrix C_{ij} is defined in (52).

In constructing the covariance matrix, when we do a combined fit to LCSR and Lattice data, we assume the matrix to be block diagonal with independent blocks for Lattice and LCSR, equivalent to $\chi^2 = \chi^2_{\text{LCSR}} + \chi^2_{\text{Lat}}$, where

$$\chi^2_{\text{LCSR}}(\vec{\theta}) = \Big(F_i - F(t_i, \vec{\theta})\Big) \left[V^{-1}_{\text{LCSR}}\right]_{ij} \Big(F_j - F(t_j, \vec{\theta})\Big) \,, \tag{54}$$

and

$$\chi^2_{\text{Lat}}(\vec{\theta}) = \Big(F_i - F(t_i, \vec{\theta})\Big) \left[V^{-1}_{\text{Lat}}\right]_{ij} \Big(F_j - F(t_j, \vec{\theta})\Big) \,, \tag{55}$$

We consider the statistical and systematic contributions to the Lattice errors separately. Where results were not available in the literature, we received the breakdown by private communication with the authors. In obtaining the covariance matrix, we make the following conservative assumptions:

- Statistical errors of Lattice data are 50% correlated [4, 7].
- Systematic errors of Lattice data are 100% correlated [4, 7].

- Errors of LCSR data are due to parametric as well as to systematic uncertainties from different sources. In order to provide a concrete number for the χ^2 value characeterizing the quality of the fit, we have estimated the errors of LCSR data at different values t_i to be 75% correlated.[7]

This prescription leads to a covariance matrix $V^{ij} = \mathrm{cov}[\mathrm{t^i}, \mathrm{t^j}]$, containing

$$V^{ij}_{\mathrm{LCSR}} = \frac{1}{4}\kappa^i\kappa^j\delta_{ij} + \frac{3}{4}\kappa^i\kappa^j \qquad \text{and} \tag{56}$$

$$V^{ij}_{\mathrm{Lat}} = \frac{1}{2}\sigma^i\sigma^j\delta_{ij} + \frac{1}{2}\sigma^i\sigma^j + \varepsilon^i\varepsilon^j \tag{57}$$

where σ_i are the statistical errors, ε_i are the systematic errors for the Lattice data, and κ_i are the errors for the LCSR predictions.

Minimising $\chi^2(\vec{\theta})$ then yields the best fit parameters $\vec{\theta}^*$, as well as the covariance matrix of the fit, $U_{ij} = \mathrm{cov}[\theta_\mathrm{i}, \theta_\mathrm{j}]$,

$$\left(U^{-1}\right)_{ij} = \frac{1}{2}\left.\frac{\partial^2\chi^2(\vec{\theta})}{\partial\theta_i\,\partial\theta_j}\right|_{\vec{\theta}=\vec{\theta}^*}, \tag{58}$$

from which we calculate the error associated to the fitted FF function:

$$\Delta F(t,\vec{\theta}^*) = \left.\frac{\partial F(t,\vec{\theta})}{\partial\theta_i}\right|_{\vec{\theta}=\vec{\theta}^*} U_{ij} \left.\frac{\partial F(t,\vec{\theta})}{\partial\theta_j}\right|_{\vec{\theta}=\vec{\theta}^*} \tag{59}$$

4.4 Results

Having established the fitting procedure, we consider FFs for the decays $B \to \rho$, $B \to K$, $B \to K^*$ and $B_s \to \phi$. We concentrate on radiative and rare semi-leptonic decays, as previously the dispersive bounds had not been calculated for the tensor current, so could not be applied to these decays. The phenomenological motivations for studying the chosen decays are as follows. First, they involve flavour changing neutral currents via e.g. electroweak penguins, so they are particularly sensitive to new physics. Secondly, the di-lepton signature can easily be detected at the LHC, and the three-body or four-body final state (for subsequent decays $K^* \to K\pi$ and $\phi \to KK$) involves many promising observables related to various angular distributions [20–22, 35, 36].

From the theoretical point of view, the $B \to V\gamma$ decay as well as the low-q^2 region of $B \to L\,\ell^+\ell^-$ transitions allow for a systematic inclusion of radiative corrections within the QCD factorization approach at leading order in the $1/m_b$ expansion [19, 37]. In this region, the transition FFs (which still determine a major part of non-perturbative input) can be obtained from LCSR estimates alone. As it has been discussed, for instance, in [38], the high-q^2 region may also be interesting in order to constrain NP contributions (notably

[7] We have checked that using 90% or 50% correlation, instead — of course — globally changes the very value of χ^2, but does not influence the optimal parameter values. A similar comment applies to the number of individual LCSR points used in the fit.

to the short-distance Wilson coefficients C_9 and C_{10}), and therefore our extrapolations of LCSR results for the tensor FFs in that region will be particularly relevant for this purpose. In the following subsection, we present the results of fitting the specific FFs to both, the SE and SSE parameterisations, using LCSR and Lattice data where appropriate as discussed in Section 4.1. For the light meson masses, we use $m_K = 494$ MeV, $m_{K^*} = 892$ MeV, $m_\rho = 776$ MeV, $m_\phi = 1.02$ GeV.

$B \to K$ form factors: In Figs. 1–5, we show the fit for the various $B \to K$ FFs, which enter, for instance, the radiative $B \to K\ell^+\ell^-$ and $B \to K\nu\bar{\nu}$ decays. We compare the result of the SE and SSE parameterisations using LCSR data, and investigate the changes when the Lattice data is included. The numerical results for the best-fit parameters of the SE and SSE fit are found in corresponding Tables 5–6. The covariance matrices for these fits can also be found in Appendix E.

Generally, both parameterisations are seen to fit the data well, and importantly, we find agreement with the Lattice predictions for $\mathcal{A}_{V,0}$ and $\mathcal{A}_{V,t}$, even when they are not included in the fit. We therefore consider our extrapolation of LCSR data for the tensor FF $\mathcal{A}_{T,0}$ to the high-q^2 region, where Lattice data does not exist, as sufficiently reliable. The quality of the fits is astonishingly good, considering the χ^2 values for only two free parameters in the expansion. The differences between the SE and SSE are only marginal, which can be traced back to the usage of the optimised value for the auxiliary parameter t_0 in (16). The dispersive bounds turn out to be far from being separated, and therefore they have only little impact on the FF fit. This observation is in line with other studies of heavy-to-light FFs in the literature, see e.g. [14, 18, 39].

In order to address the question of potential contributions from higher-order terms in the SE, we consider the LCSR prediction for the vector and tensor form factors $\mathcal{A}_{V,0}$, $\mathcal{A}_{T,0}$ and fit to a SE with $K = 3$, where the coefficient a_2 of the z^2 term in the expansion has been fixed to values between $[-0.9, +0.9]$, representing almost the maximal range allowed by the unitarity constraints. The results of these fits are shown in Figs. 2,6. Let us first consider the case, where only LCSR data is used in the fit. We observe that — as expected — the constraints from the LCSR points at low values of q^2 are not sufficient to determine the behaviour at large q^2, if higher-order terms in the SE (with no further phenomenological constraints) are allowed for. However, the behaviour of the form factor corresponding to the extreme values of a_2 does not appear very realistic (even a rough numerical estimate of coupling constants for the first low-lying resonances with the considered hadronic transition would be sufficient to exclude the curves at the margin). Therefore the associated error estimate appears too pessimistic to us. Moreover, typically, exclusive semi-leptonic branching fractions are suppressed relative to the inclusive ones by a factor of about 20. This suggests that the right-hand side of the dispersive bounds should not exceed a value of 5% (instead of 100%). Correspondingly, a realistic range of allowed a_2–values should rather be taken as $[-0.25, +0.25]$, which is indicated by the thick central lines in Fig. 2. The associated uncertainty is only slightly larger than the one obtained from the variation of (a_0, a_1) for the SE fit with $K = 2$. If, on the other hand, the lattice

information (in the case of $\mathcal{A}_{V,0}$) is taken into account, the cases with $|a_2| \gtrsim 0.25$ actually do not yield a satisfactoring fit anymore, and again the error estimate of the linear fit seems to be sufficient to estimate the fit errors. In view of the generic difficulties in estimating systematic theoretical uncertainties, we thus consider the SE/SSE parameterisation with $K = 2$ and the associated error estimates as sufficiently reliable for practical applications.

Another comment applies to the scalar FFs $\mathcal{A}_{V,t}$: As shown in Table 1, the combined heavy-quark/chiral-symmetry limit considered in [26] predicts a scalar B_s resonance *below* BK-production threshold (such a state is also favoured by a Lattice computation in [40]). On the other hand, the PDG only finds resonances at masses near/above the production threshold. We have therefore chosen to compare two variants of the fit, with/without a scalar resonance.[8] As can be seen, the fit *with* a scalar resonance from [26] describes the combined Lattice/LCSR data significantly better than the fit without a low-lying resonance (where in the latter case again the dispersive bounds constrain the FF to lie systematically below the Lattice data). However, within the present uncertainties of Lattice and LCSR data, this could only be taken as a very indirect argument in favour of a scalar resonance in the anticipated mass region.

Table 5: $B \to K$: Fit of SE parameterisation to LCSR or LCSR/Lattice results, for $\mathcal{A}_{V,0}$ ($X = 1$), $\mathcal{A}_{V,t}$ ($X = 3$) and $\mathcal{A}_{T,0}$ ($X = 1$).

A_X	m_R	α_0	α_1	Fit to	$\chi^2_{\rm fit}$	$X\sum_i \alpha_i^2$
$\mathcal{A}_{V,0}$	5.41	-2.5×10^{-2}	7.2×10^{-2}	LCSR and Lattice	0.329	5.77×10^{-3}
$\mathcal{A}_{V,t}$	-	-6.8×10^{-2}	0.20	LCSR and Lattice	0.200	0.129
$\mathcal{A}_{V,t}$	5.72	-4.5×10^{-2}	8.9×10^{-2}	LCSR and Lattice	0.234	2.99×10^{-2}
$\mathcal{A}_{V,0}$	5.41	-2.4×10^{-2}	6.2×10^{-2}	LCSR	5.07×10^{-3}	4.43×10^{-3}
$\mathcal{A}_{V,t}$	-	-6.7×10^{-2}	0.18	LCSR	1.44×10^{-3}	0.111
$\mathcal{A}_{V,t}$	5.72	-4.8×10^{-2}	0.11	LCSR	1.54×10^{-4}	4.34×10^{-2}
$\mathcal{A}_{T,0}$	5.41	-2.8×10^{-2}	6.0×10^{-2}	LCSR	3.94×10^{-3}	4.40×10^{-3}

[8] Notice that BZ [8] use an effective resonance mass above production threshold to parameterise the scalar FFs.

Table 6: $B \to K$: Fit of SSE parameterisation to LCSR or LCSR/Lattice results, for $\mathcal{A}_{V,0}$ ($X = 1$), $\mathcal{A}_{V,t}$ ($X = 3$) and $\mathcal{A}_{T,0}$ ($X = 1$).

A_X	m_R	$\tilde{\alpha}_0$	$\tilde{\alpha}_1$	Fit to	χ^2_{fit}	$X \sum_{i,j} C_{i,j}\tilde{\alpha}_i\tilde{\alpha}_j$
$\mathcal{A}_{V,0}$	5.41	0.50	-1.4	LCSR and Lattice	0.940	6.51×10^{-3}
$\mathcal{A}_{V,t}$	-	0.54	-1.7	LCSR and Lattice	0.904	0.142
$\mathcal{A}_{V,t}$	5.72	0.28	0.35	LCSR and Lattice	0.128	3.15×10^{-2}
$\mathcal{A}_{V,0}$	5.41	0.48	-1.0	LCSR	5.15×10^{-3}	4.04×10^{-3}
$\mathcal{A}_{V,t}$	-	0.52	-1.4	LCSR	2.27×10^{-3}	9.55×10^{-2}
$\mathcal{A}_{V,t}$	5.72	0.30	0.20	LCSR	7.17×10^{-5}	5.32×10^{-2}
$\mathcal{A}_{T,0}$	5.41	0.48	-1.1	LCSR	8.15×10^{-3}	3.06×10^{-3}

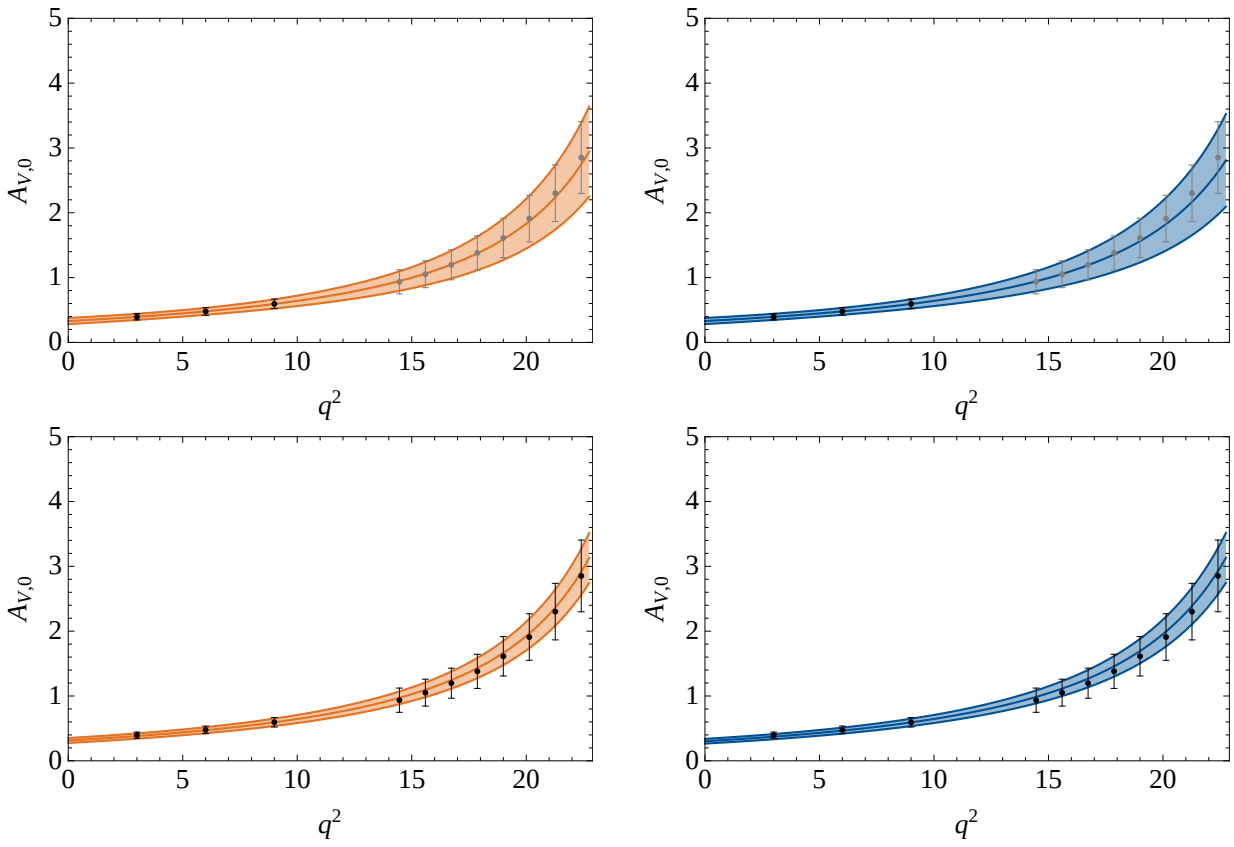

Figure 1: $B \to K$: Fit of SE (left) and SSE (right) parameterisation to LCSR (top) and to LCSR and Lattice (bottom) for $\mathcal{A}_{V,0}$. The LCSR and Lattice data are shown by black points with error bars in the appropriate q^2 range.

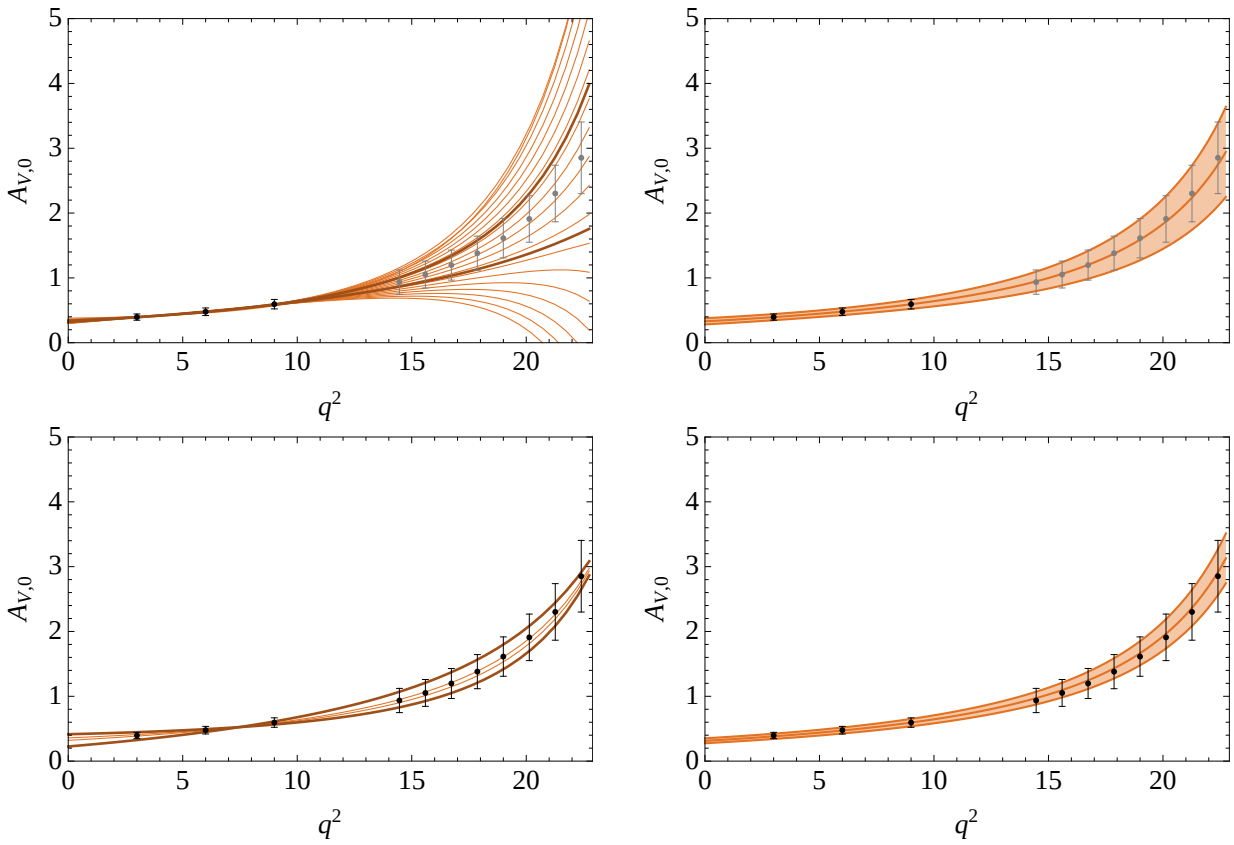

Figure 2: $B \to K$: Fit of SE parameterisation to LCSR or LCSR/Lattice for $\mathcal{A}_{V,0}$ with the parameter a_2 varied between $[-0.9, +0.9]$ (thin lines). The thick, dark lines show $a_2 = \pm 0.25$. For comparison, on the right we show again the corresponding fit and error estimate for a SE truncated after a_1.

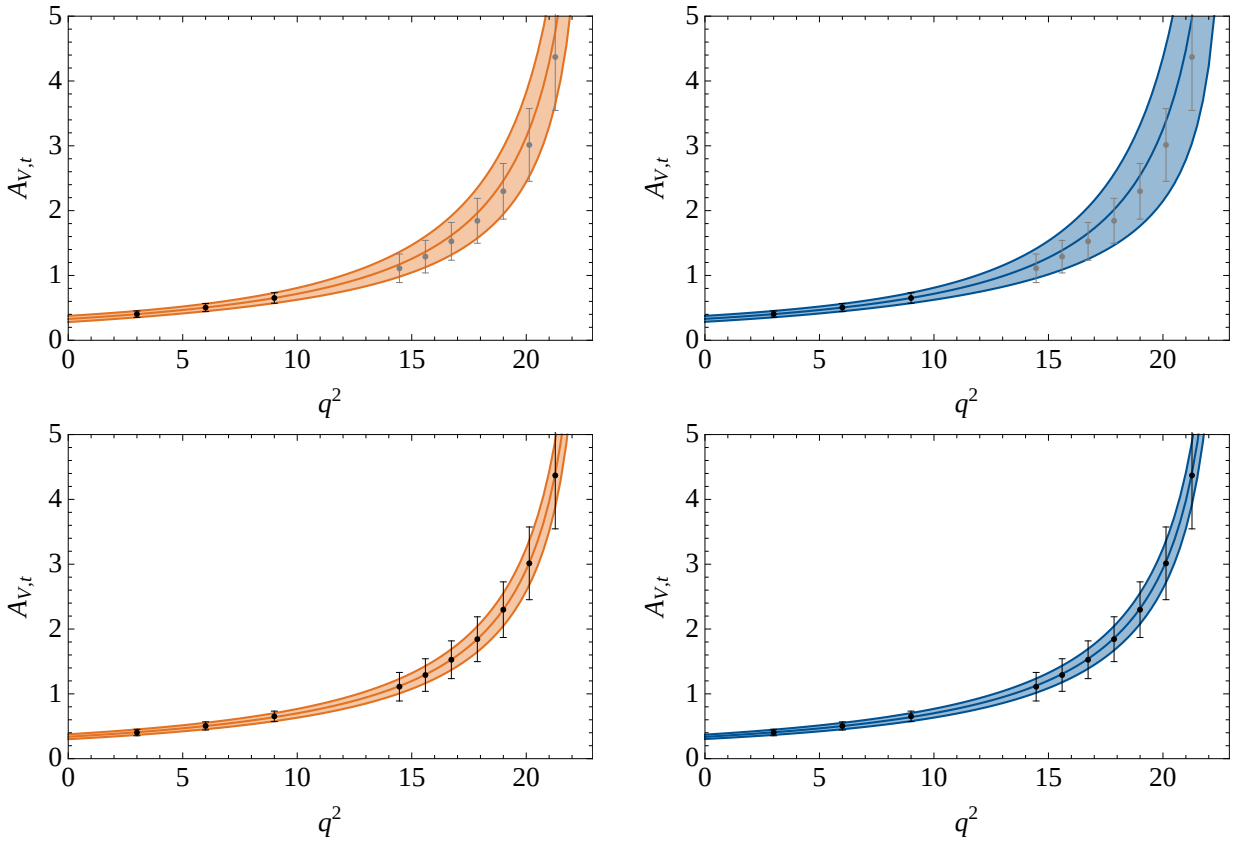

Figure 3: $B \to K$: Fit of SE (left) and SSE (right) parameterisations to LCSR (top) and to LCSR and Lattice (bottom) for $\mathcal{A}_{V,t}$. The LCSR and Lattice data are shown by black points with error bars in the appropriate q^2 range.

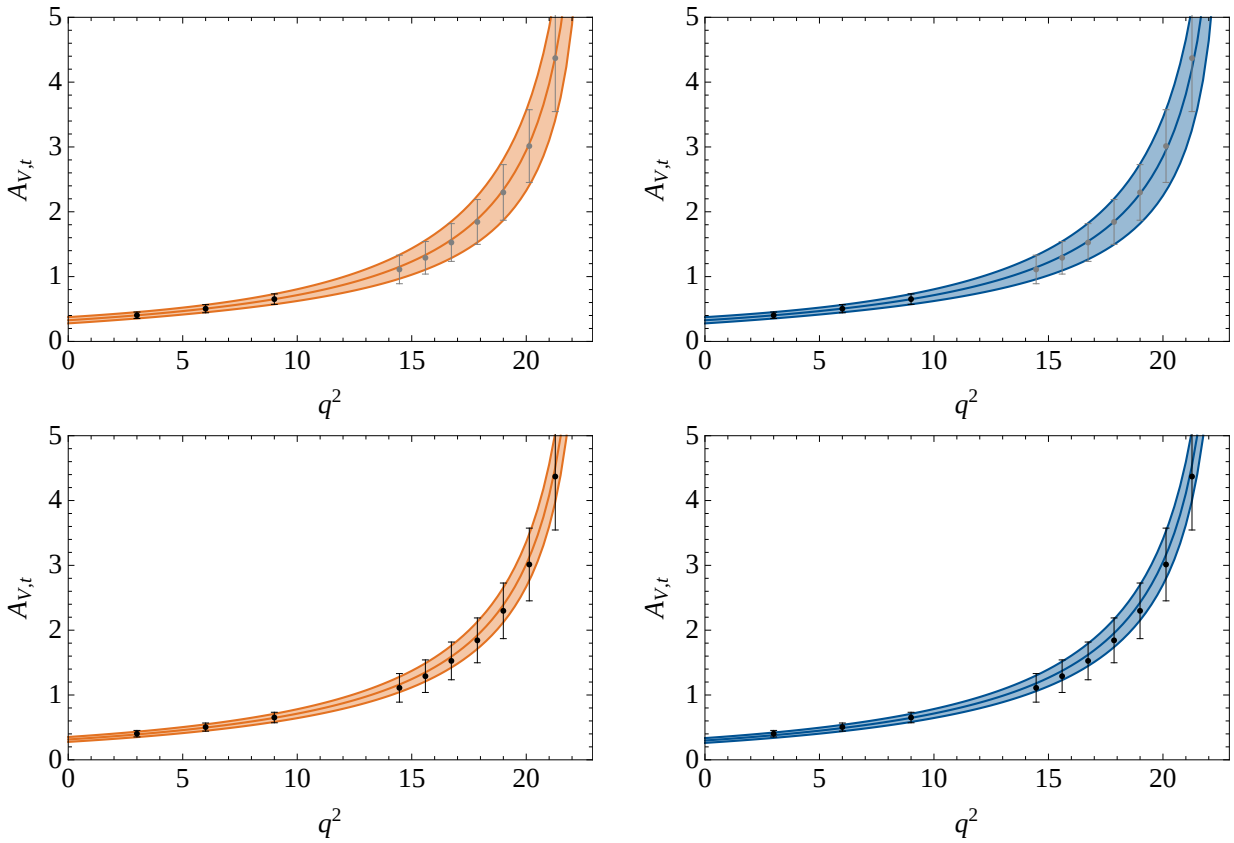

Figure 4: $B \to K$: The same as Fig. 3 but without using the scalar B_s resonance in the fit ansatz.

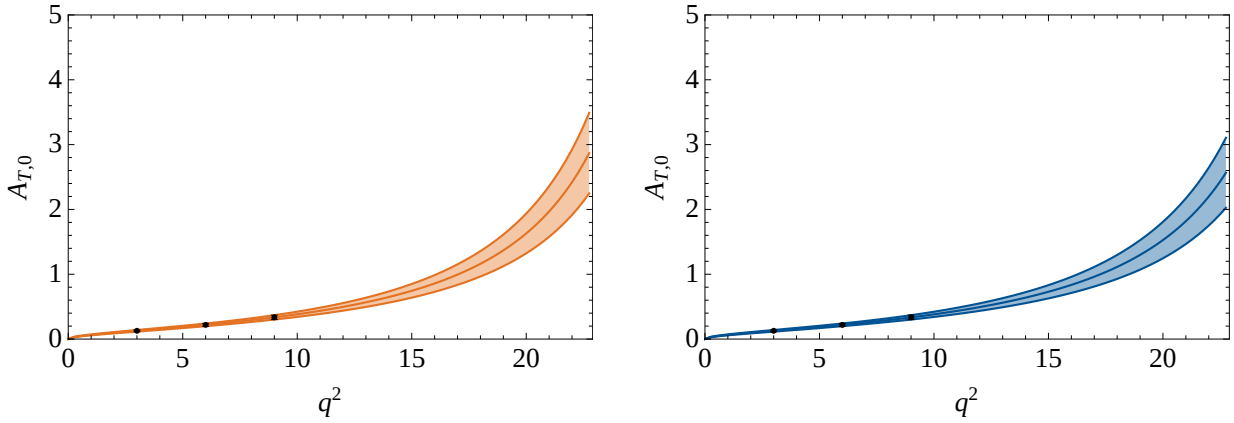

Figure 5: $B \to K$: Fit of SE (left) and SSE (right) parameterisations to LCSR for $\mathcal{A}_{T,0}$. The LCSR data is shown by black points with error bars.

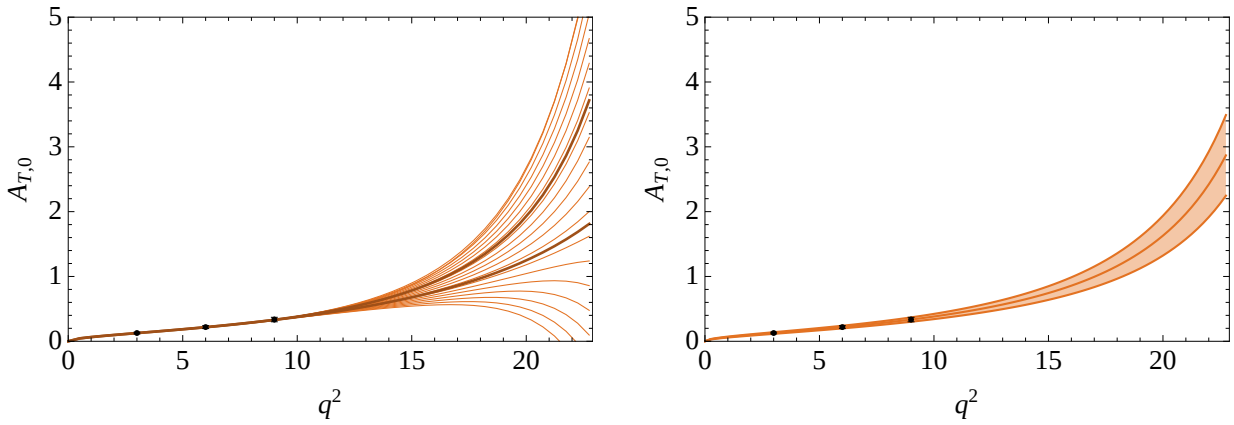

Figure 6: Same as Fig. 2, but for $\mathcal{A}_{T,0}$ (no lattice data).

$B \to \rho$ form factors: Our FF fits for $B \to \rho$ transitions, relevant for the radiative $B \to \rho\gamma$ and $B \to \rho\ell^+\ell^-$ decays, are summarized in Figs. 7–13 and Tables 7 and 8, where we again compare the fit to SE and SSE parameterisations. As in the case of $B \to K$ FFs, we generally observe similar good results for SE and SSE fits, with the dispersive bounds again playing only a minor role in restricting the coefficients of the SE/SSE. The covariance matrices for the fits can again be found in Appendix E.

Lattice results are restricted to the (axial–)vector FFs, and we again study how the fits change when the Lattice data is included: In case of the FF $\mathcal{B}_{V,0}$, the uncertainties on the Lattice data are rather large, and the fit is in any case dominated by the LCSR points at low values of q^2. Still, we find that the best-fit curve also well describes the central values of the Lattice estimates. The situation is somewhat different for $\mathcal{B}_{V,1}$, where the central values of the Lattice points do not quite agree with the extrapolation of the LCSR prediction. The fit is consistent within Lattice uncertainties, but a rather large value of χ^2, dominated by the deviations from the Lattice points, is generated. On the other hand, for $\mathcal{B}_{V,1}$ the Lattice data are competitive with the LCSR input, and we can again observe that the extrapolation of the LCSR predictions describes the Lattice points very well, while inclusion of the Lattice data in this case leads to a very precise FF description.

In the remaining cases, we again provide the extrapolations for the pseudoscalar and tensor FFs from LCSR input, where Lattice data have not been available. Here, it is to be mentioned that the uncertainties for the FF $\mathcal{B}_{T,0}$ are quite large, because we had to determine the LCSR input values from the *difference* of two FFs in (12). Of course, it would be desirable to directly calculate the FF $\mathcal{B}_{T,0}$ in the LCSR approach which should lead to significantly smaller uncertainties for the input data and the extrapolation to large values of q^2. A similar comment applies to the FF $\mathcal{B}_{V,0}$.

Table 7: $B \to \rho$: Fit of SE parameterisation to LCSR or LCSR/Lattice results for $\mathcal{B}_{V,0-2}$ ($X = 1$), $\mathcal{B}_{V,t}$ ($X = 3$) and $\mathcal{B}_{T,0-2}$ ($X = 1$).

B_X	m_R	β_0	β_1	Fit to	$\chi^2_{\rm fit}$	$X\sum_i \beta_i^2$
$\mathcal{B}_{V,0}$	5.72	-8.0×10^{-3}	2.5×10^{-2}	LCSR and Lattice	32.1	1.98×10^{-2}
$\mathcal{B}_{V,1}$	5.33	-3.5×10^{-2}	0.11			
$\mathcal{B}_{V,2}$	5.72	-2.5×10^{-2}	7.8×10^{-2}			
$\mathcal{B}_{V,0}$	5.72	-7.5×10^{-3}	1.4×10^{-2}	LCSR	9.56×10^{-2}	1.28×10^{-2}
$\mathcal{B}_{V,1}$	5.33	-3.7×10^{-2}	8.9×10^{-2}			
$\mathcal{B}_{V,2}$	5.72	-2.3×10^{-2}	5.2×10^{-2}			
$\mathcal{B}_{V,t}$	5.28	-3.2×10^{-2}	8.9×10^{-2}	LCSR	3.81×10^{-3}	2.66×10^{-2}
$\mathcal{B}_{T,0}$	5.72	-1.4×10^{-2}	-8.3×10^{-3}	LCSR	4.18×10^{-2}	1.86×10^{-3}
$\mathcal{B}_{T,1}$	5.33	-1.0×10^{-2}	3.4×10^{-2}			
$\mathcal{B}_{T,2}$	5.72	-6.3×10^{-3}	1.7×10^{-2}			

Table 8: $B \to \rho$: Fit of SSE parameterisation to LCSR or LCSR/Lattice results for $\mathcal{B}_{V,0-2}$ ($X = 1$), $\mathcal{B}_{V,t}$ ($X = 3$) and $\mathcal{B}_{T,0-2}$ ($X = 1$).

B_X	m_R	$\tilde{\beta}_0$	$\tilde{\beta}_1$	Fit to	$\chi^2_{\rm fit}$	$X\sum_{i,j} C_{i,j}\tilde{\beta}_i\tilde{\beta}_j$
$\mathcal{B}_{V,0}$	5.72	0.26	0.14	LCSR and Lattice	33.0	1.85×10^{-2}
$\mathcal{B}_{V,1}$	5.33	0.51	-1.7			
$\mathcal{B}_{V,2}$	5.72	0.40	-0.15			
$\mathcal{B}_{V,0}$	5.72	0.26	0.50	LCSR	4.34×10^{-2}	1.10×10^{-2}
$\mathcal{B}_{V,1}$	5.33	0.54	-1.4			
$\mathcal{B}_{V,2}$	5.72	0.37	0.24			
$\mathcal{B}_{V,t}$	5.28	0.43	-1.3	LCSR	8.49×10^{-3}	2.16×10^{-2}
$\mathcal{B}_{T,0}$	5.72	0.35	0.94	LCSR	3.57×10^{-2}	1.79×10^{-3}
$\mathcal{B}_{T,1}$	5.33	0.52	-1.5			
$\mathcal{B}_{T,2}$	5.72	0.34	0.31			

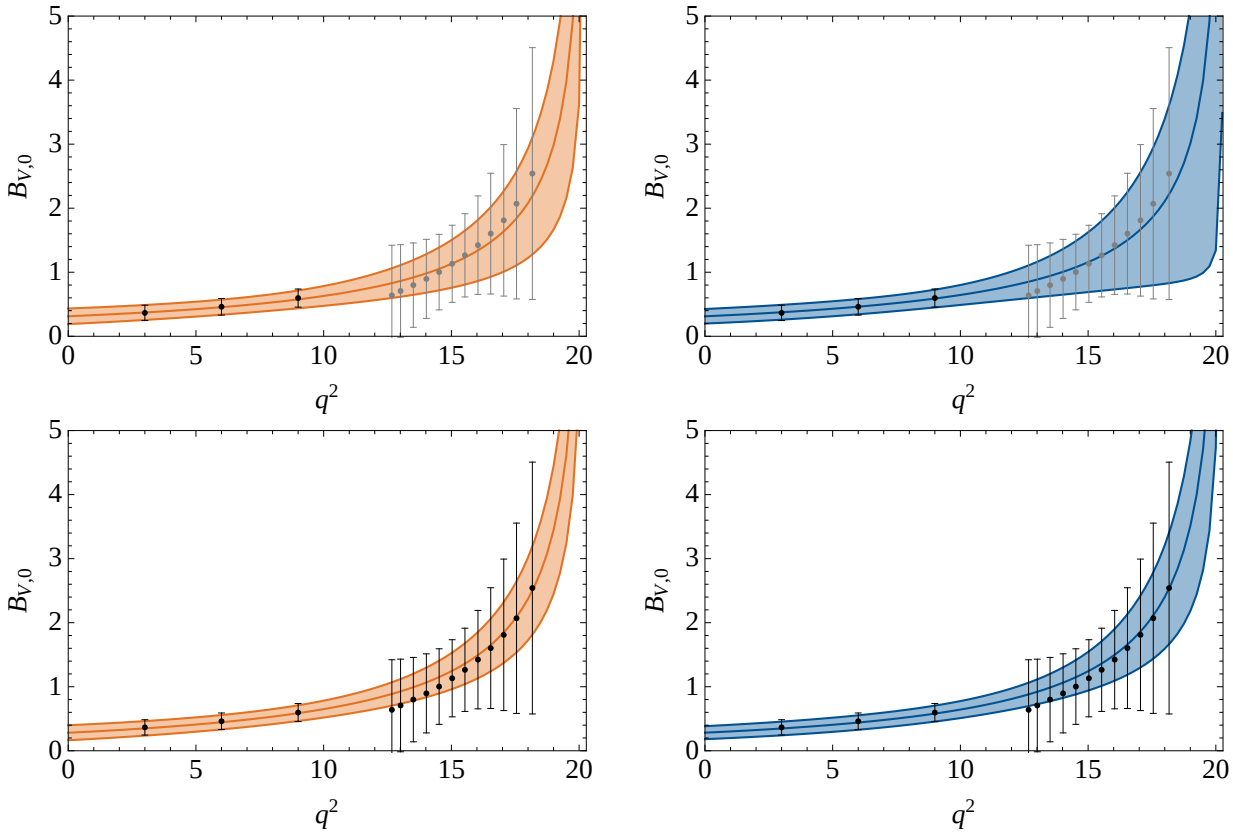

Figure 7: $B \to \rho$: Fit of SE (left) and SSE (right) parameterisations to LCSR (top) and to LCSR and Lattice (bottom) for $\mathcal{B}_{V,0}$. The LCSR and Lattice data are shown by black points with error bars in the appropriate q^2 range.

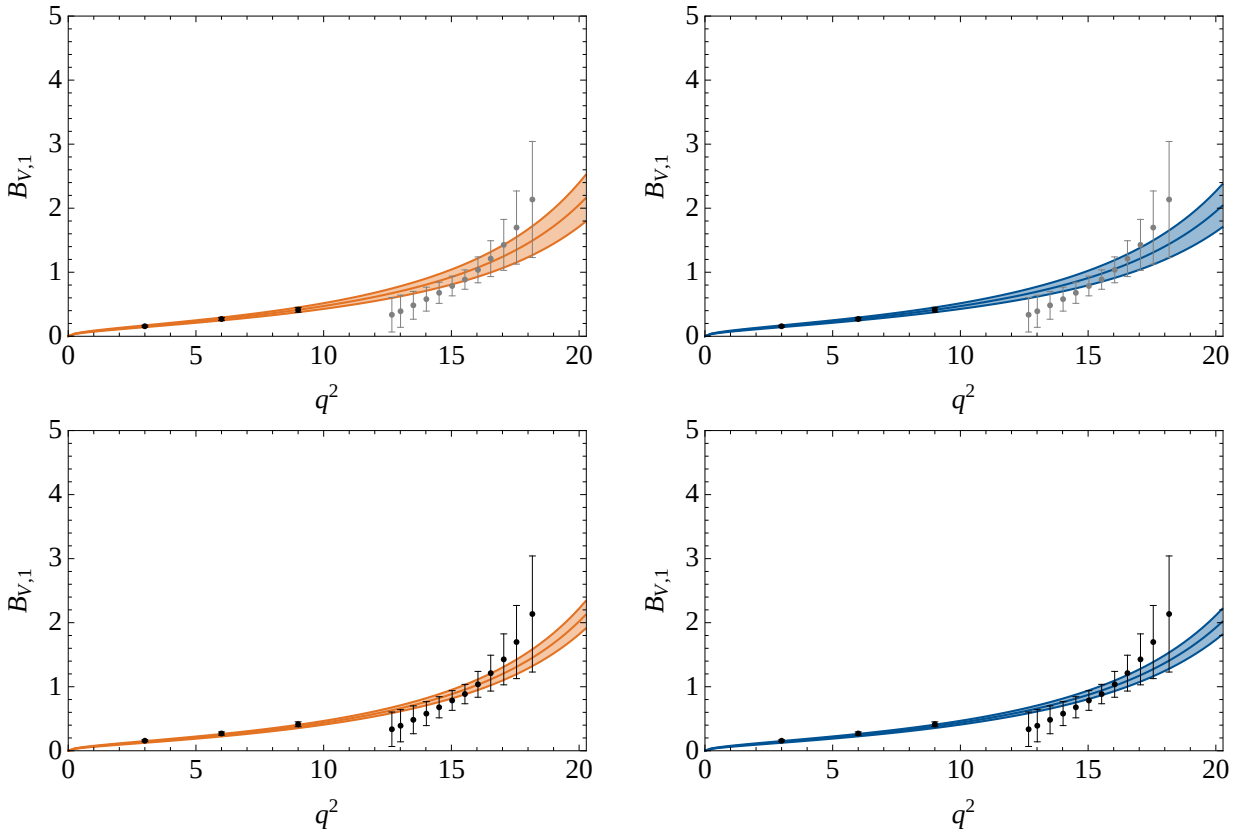

Figure 8: $B \to \rho$: Fit of SE (left) and SSE (right) parameterisations to LCSR (top) and to LCSR and Lattice (bottom) for $\mathcal{B}_{V,1}$. The LCSR and Lattice data are shown by black points with error bars in the appropriate q^2 range.

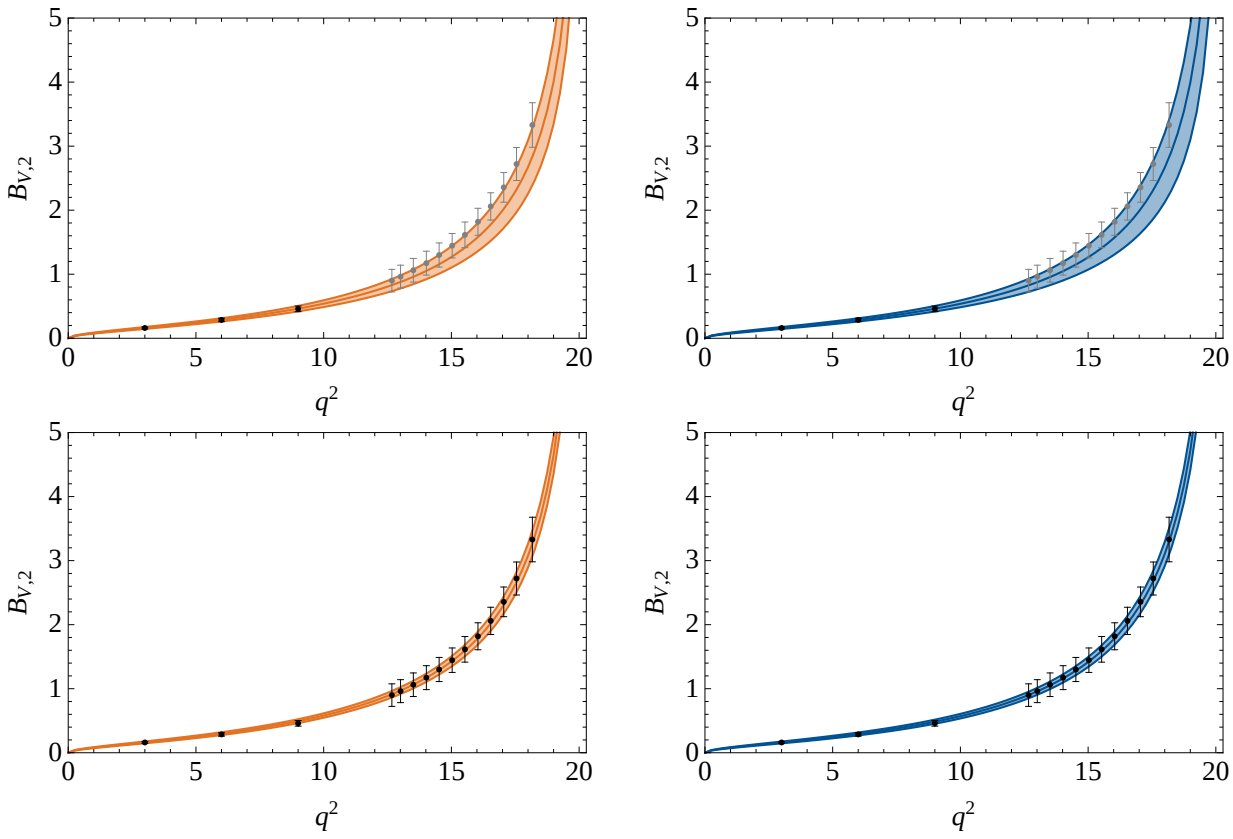

Figure 9: $B \to \rho$: Fit of SE (left) and SSE (right) parameterisations to LCSR (top) and to LCSR and Lattice (bottom) for $\mathcal{B}_{V,2}$. The LCSR and Lattice data are shown by black points with error bars in the appropriate q^2 range.

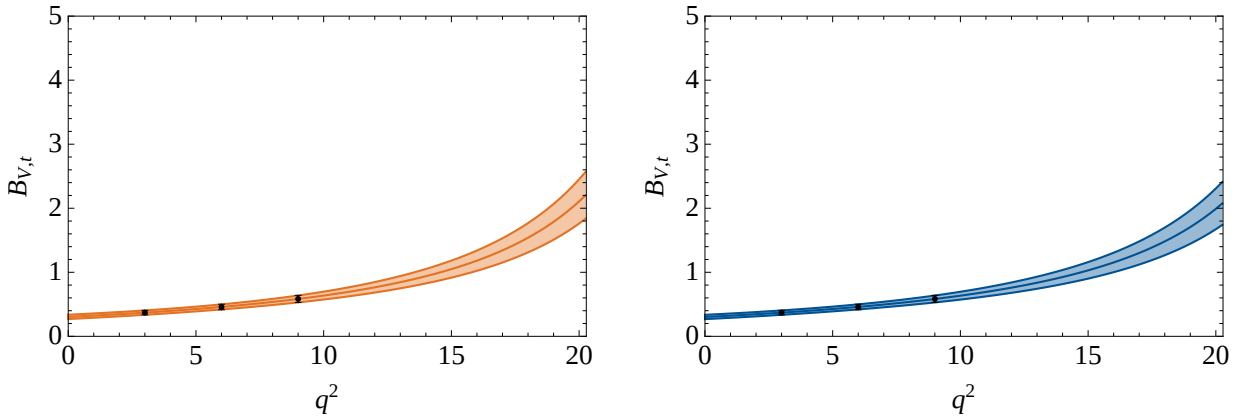

Figure 10: $B \to \rho$: Fit of SE (left) and SSE (right) parameterisations to LCSR for $\mathcal{B}_{V,t}$. The LCSR data is shown by black points with error bars.

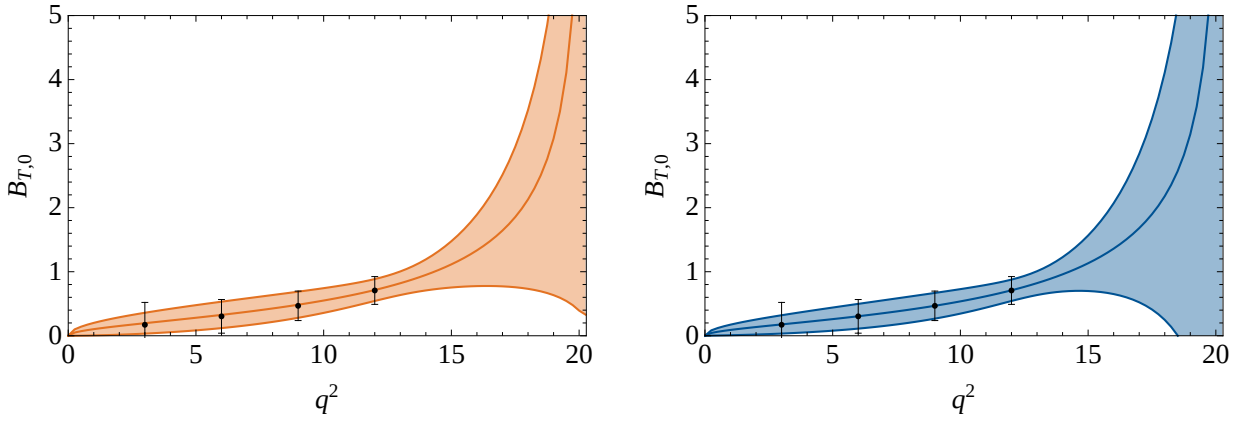

Figure 11: $B \to \rho$: Fit of SE (left) and SSE (right) parameterisations to LCSR for $\mathcal{B}_{T,0}$. The LCSR data is shown by black points with error bars.

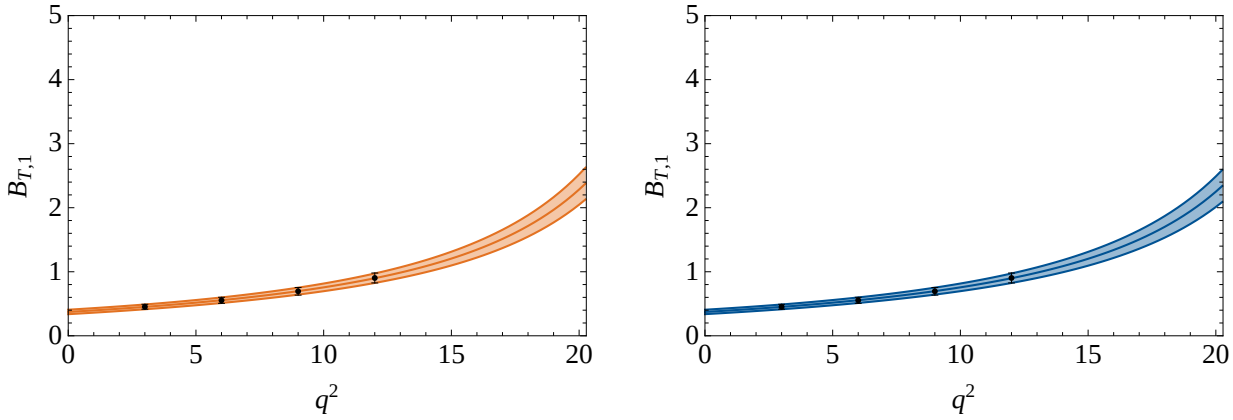

Figure 12: $B \to \rho$: Fit of SE (left) and SSE (right) parameterisations to LCSR for $\mathcal{B}_{T,1}$. The LCSR data is shown by black points with error bars.

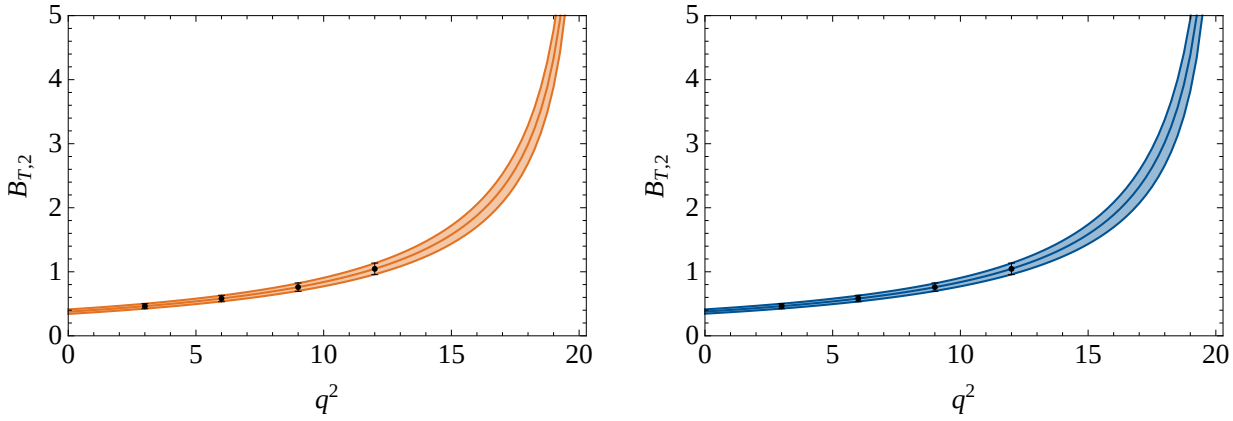

Figure 13: $B \to \rho$: Fit of SE (left) and SSE (right) parameterisations to LCSR for $\mathcal{B}_{T,2}$. The LCSR data is shown by black points with error bars.

$B \to K^*$ and $B_s \to \phi$ form factors: The analysis of $B \to K^*$ transitions is more difficult on the Lattice, as the K^*–meson is unstable. Quenched calculations on the Lattice have been attempted for the tensor FFs needed in $B \to K^*\gamma$, at $q^2 = 0$, but we do not include these results in our analysis as the other FFs for this decay have not so far been calculated. Therefore, we can only fit to the LCSR data, and our numerical results for the best-fit parameters of the SE and SSE fit are found in Tables 9 and 10. The covariance matrices for the fits can also be found in Appendix E.

Table 9: $B \to K^*$: Fit of SE parameterisation to LCSR results for $\mathcal{B}_{V,0-2}$ $(X = 1)$, $\mathcal{B}_{V,t}$ $(X = 3)$ and $\mathcal{B}_{T,0-2}$ $(X = 1)$.

B_X	m_R	β_0	β_1	Fit to	$\chi^2_{\rm fit}$	$X\sum_i \beta_i^2$
$\mathcal{B}_{V,0}$	5.83	-9.4×10^{-3}	1.4×10^{-2}			
$\mathcal{B}_{V,1}$	5.41	-5.0×10^{-2}	0.10	LCSR	0.149	1.86×10^{-2}
$\mathcal{B}_{V,2}$	5.83	-3.0×10^{-2}	6.8×10^{-2}			
$\mathcal{B}_{V,t}$	5.37	-4.4×10^{-2}	0.11	LCSR	1.72×10^{-3}	4.25×10^{-2}
$\mathcal{B}_{T,0}$	5.83	-1.9×10^{-2}	-1.9×10^{-2}			
$\mathcal{B}_{T,1}$	5.41	-1.4×10^{-2}	4.1×10^{-2}	LCSR	1.88×10^{-2}	3.14×10^{-3}
$\mathcal{B}_{T,2}$	5.83	-8.0×10^{-3}	2.2×10^{-2}			

As in the case of $B \to K^*$, Lattice QCD predictions for $B_s \to \phi$ FFs are lacking, and we fit to the LCSR data, only. Our numerical results for the best-fit parameters of the SE and SSE parameterisations are found in Tables 11 and 12. The covariance matrices for the fits can also be found in Appendix E. In all cases, we find a good description of the LCSR input at low q^2, and from the experience in $B \to K$ and $B \to \rho$ transitions we expect the extrapolation to high q^2 to be sufficiently reliable. Still, input from Lattice computations – if feasible – for $B \to K^*$ and $B_s \to \phi$ transitions at intermediate values of q^2 would be highly welcome.

Table 10: $B \to K^*$: Fit of SSE parameterisation to LCSR results for $\mathcal{B}_{V,0-2}$ ($X = 1$), $\mathcal{B}_{V,t}$ ($X = 3$) and $\mathcal{B}_{T,0-2}$ ($X = 1$).

B_X	m_R	$\tilde{\beta}_0$	$\tilde{\beta}_1$	Fit to	χ^2_{fit}	$X \sum_{i,j} C_{i,j}\tilde{\beta}_i\tilde{\beta}_j$
$\mathcal{B}_{V,0}$	5.83	0.31	0.74			
$\mathcal{B}_{V,1}$	5.41	0.62	-1.4	LCSR	5.84×10^{-2}	1.63×10^{-2}
$\mathcal{B}_{V,2}$	5.83	0.45	0.35			
$\mathcal{B}_{V,t}$	5.37	0.49	-1.4	LCSR	4.63×10^{-3}	3.62×10^{-2}
$\mathcal{B}_{T,0}$	5.83	0.45	1.4			
$\mathcal{B}_{T,1}$	5.41	0.60	-1.5	LCSR	9.65×10^{-3}	2.75×10^{-3}
$\mathcal{B}_{T,2}$	5.83	0.42	0.45			

Table 11: $B_s \to \phi$: Fit of SE parameterisation to LCSR results for $\mathcal{B}_{V,0-2}$ ($X = 1$), $\mathcal{B}_{V,t}$ ($X = 3$) and $\mathcal{B}_{T,0-2}$ ($X = 1$).

B_X	m_R	β_0	β_1	Fit to	χ^2_{fit}	$X \sum_i \beta_i^2$
$\mathcal{B}_{V,0}$	5.83	-5.8×10^{-3}	3.5×10^{-3}			
$\mathcal{B}_{V,1}$	5.41	-3.4×10^{-2}	9.6×10^{-2}	LCSR	0.124	1.29×10^{-2}
$\mathcal{B}_{V,2}$	5.83	-1.8×10^{-2}	4.7×10^{-2}			
$\mathcal{B}_{V,t}$	5.37	-3.4×10^{-2}	9.3×10^{-2}	LCSR	8.93×10^{-3}	2.96×10^{-2}
$\mathcal{B}_{T,0}$	5.83	-1.1×10^{-2}	-1.5×10^{-2}			
$\mathcal{B}_{T,1}$	5.41	-9.0×10^{-3}	3.5×10^{-2}	LCSR	4.45×10^{-2}	1.86×10^{-3}
$\mathcal{B}_{T,2}$	5.83	-4.6×10^{-3}	1.4×10^{-2}			

Table 12: $B_s \to \phi$: Fit of SSE parameterisation to LCSR results for $\mathcal{B}_{V,0-2}$ ($X = 1$), $\mathcal{B}_{V,t}$ ($X = 3$) and $\mathcal{B}_{T,0-2}$ ($X = 1$).

B_X	m_R	$\tilde{\beta}_0$	$\tilde{\beta}_1$	Fit to	χ^2_{fit}	$X \sum_{i,j} C_{i,j}\tilde{\beta}_i\tilde{\beta}_j$
$\mathcal{B}_{V,0}$	5.83	0.37	1.1			
$\mathcal{B}_{V,1}$	5.41	0.67	-2.1	LCSR	1.44×10^{-2}	1.15×10^{-2}
$\mathcal{B}_{V,2}$	5.83	0.50	0.19			
$\mathcal{B}_{V,t}$	5.37	0.61	-1.8	LCSR	1.57×10^{-2}	2.58×10^{-2}
$\mathcal{B}_{T,0}$	5.83	0.51	1.7			
$\mathcal{B}_{T,1}$	5.41	0.66	-2.2	LCSR	3.49×10^{-2}	1.66×10^{-3}
$\mathcal{B}_{T,2}$	5.83	0.46	0.26			

5 Discussion and Conclusions

We have shown that the form factors (FFs) relevant for radiative and semi-leptonic decays of B and B_s mesons into light pseudoscalar or vector mesons can be conveniently parameterised as a series expansion (SE) in the variable $z(t)$ (see the definition in (15)). With the current accuracy of theoretical estimates from light-cone sum rules (LCSRs) and (where available) Lattice QCD, we found that keeping only two terms in the expansion and correctly implementing the analytical behaviour due to below-threshold resonances, results in a very good description of the FFs over the whole range of momentum transfer in the physical decay region.

The coefficients of the SE are further constrained by dispersive bounds, exploiting the crossing symmetry between the physical B-meson decay and the pair-production of heavy and light mesons by the considered decay current. In order to put the discussion for the various FFs on a common footing, we found it convenient to use a FF basis where the decay/production currents are projected by transverse, longitudinal and time-like polarisation vectors with respect to momentum transfer t. Considering the corresponding projections for the current correlators, the constraints take the simple form as indicated in (46,47). We stress that for decays into vector mesons the dispersive bounds constrain the *sum* of (squared) coefficients for the three axial-vector FFs, as well as for the three tensor FFs. In a simultaneous fit of all FFs, these constraints are thus stronger than those for the individual FFs in that sum.

In order to determine the correct normalization of the SE, given by the profile functions $\phi(z(t))$, we calculate the current correlators using an OPE, including NLO perturbative corrections and the leading non-perturbative contributions from quark, gluon and mixed condensates. In particular, we provide the NLO results for the tensor-current correlation functions, which are relevant for the FFs appearing in radiative and rare semi-leptonic B

decays.

With these theoretical tools at hand, we have performed numerical fits to LCSR (Lattice) predictions at low (medium) momentum transfer for all the FFs appearing in $B \to K, \rho, K^*$ and $B_s \to \phi$ transitions. We have also investigated a simplified form of the SE, where the profile functions $\phi(z(t))$ are re-expanded in powers of $z(t)$, while the dispersive bounds take a somewhat more complicated form. We find that both the standard and the simplified SE give a similarly good description of the FF functions. In those cases, where Lattice estimates of the FFs is lacking, the SE is used to extrapolate the LCSR predictions to the high-q^2 region. Comparing fits with/without using the available Lattice data for $B \to K$ and $B \to \rho$ transitions, we judge these extrapolations to be rather reliable. Some of our results could be further improved in the future, by addressing some of the following issues: The experimental confirmation of a scalar B_s resonance below B–K threshold, contributing to the scalar $B \to K$ FF. Decreasing the uncertainties in Lattice predictions for $B \to \rho$ axial-vector FFs. The calculation of LCSRs directly in the helicity basis. The reliable computation of $B \to K^*$ and $B_s \to \phi$ FFs on the Lattice.

In conclusion, we have shown that the parameterisation of heavy-to-light FFs as a (truncated) SE in $z(t)$ in combination with theoretical estimates from LCSRs and Lattice QCD is very useful, not only for the determination of the CKM element $|V_{ub}|$ from charged semi-leptonic $B \to \pi$ or $B \to \rho$ decays, but also for the description of FFs for radiative and semi-leptonic $b \to s$ and $b \to d$ transitions, which will continue to play a major role for the indirect search of new physics effects from rare flavour decays.

Acknowledgements

AKMB is very grateful to her supervisor Patricia Ball for many helpful discussions, and also acknowledges an STFC studentship.

A Kinematics and Polarization Vectors

In the following, we consider the rest frame of the decaying B-meson, with the 3-momentum of the final-state meson pointing in the z-direction. The polarisation vectors for a (virtual) vector state, with 4-momentum $q^\mu = (q^0, 0, 0, -|\vec{q}\,|)$, are defined as

$$\begin{aligned} \varepsilon_\pm^\mu(q) &= \mp\frac{1}{\sqrt{2}}\,(0, 1, \mp i, 0)\,, \qquad \varepsilon_0^\mu(q) = \frac{1}{\sqrt{q^2}}\,(|\vec{q}\,|, 0, 0, -q^0)\,, \\ \varepsilon_t^\mu(q) &= \frac{1}{\sqrt{q^2}}\,q^\mu\,. \end{aligned} \tag{60}$$

For the decay of a B-meson at rest into a light meson with mass m_L and momentum $\vec{k}$, we have in particular

$$q^0 = m_B - E = \frac{m_B^2 - m_L^2 + q^2}{2m_B}\,, \qquad |\vec{q}\,| = |\vec{k}\,| = \frac{\sqrt{\lambda}}{2m_B}\,, \tag{61}$$

with λ defined in (6). We also define the linear combinations

$$\varepsilon_1^\mu(q) \;=\; \frac{\varepsilon_-^\mu(q)-\varepsilon_+^\mu(q)}{\sqrt{2}} = (0,1,0,0)\,, \qquad \varepsilon_2^\mu(q) = \frac{\varepsilon_-^\mu(q)+\varepsilon_+^\mu(q)}{\sqrt{2}} = (0,0,i,0)\,. \quad (62)$$

In the same way, the polarisation vectors for an on-shell K^* meson with momentum $k^\mu = (E,0,0,|\vec{k}\,|)$ are given as

$$\varepsilon_\pm^\mu(k) \;=\; \mp\frac{1}{\sqrt{2}}(0,1,\pm i,0)\,, \qquad \varepsilon_0^\mu(k) = \frac{1}{m_{K^*}}(|\vec{k}\,|,0,0,E)\,. \quad (63)$$

B FF Properties

In the following, we summarize a few useful properties of the helicity-based FFs, following from the definitions in (5,8,10,12). From the e.o.m. for vanishing momentum transfer, $q^2 \to 0$, one derives

$$\mathcal{A}_{V,0}(0) = \mathcal{A}_{V,t}(0) = f_0(0) = f_+(0)\,, \quad (64)$$

and

$$\begin{aligned}\mathcal{B}_{V,0}(0) &= \mathcal{B}_{V,t}(0) = A_0(0) = A_3(0)\,,\\ \mathcal{B}_{T,1}(0) &= \mathcal{B}_{T,2}(0) = \sqrt{2}\,T_1(0) = \sqrt{2}\,T_2(0)\,,\end{aligned} \quad (65)$$

while the FFs $\mathcal{A}_{T,0}$, $\mathcal{B}_{V,1}$, $\mathcal{B}_{V,2}$, and $\mathcal{B}_{T,0}$ vanish like $\sqrt{q^2}$. Similarly, at the kinematic endpoint $q^2 = t_- = (m_B - m_L)^2$, we obtain the relations

$$\lim_{q^2\to t_-}\frac{\mathcal{B}_{V,2}(q^2)}{\mathcal{B}_{V,0}(q^2)} = \lim_{q^2\to t_-}\frac{\mathcal{B}_{T,2}(q^2)}{\mathcal{B}_{T,0}(q^2)} = \sqrt{2}\,, \quad (66)$$

which has been implemented in our FF parameterisation in Section 4.3.

In the infinite-mass limit $m_b \to \infty$, one can project the heavy quark field in the decay current onto its large component in HQET, which results in the well-known HQET spin-symmetry relations. With our FF conventions, they read

$$2m_B\sqrt{q^2}\,\mathcal{A}_{T,0} = (m_B^2+q^2)\,\mathcal{A}_{V,0} - (m_B^2-q^2)\,\mathcal{A}_{V,t}\,, \quad (67)$$

and

$$\begin{aligned}2m_B\sqrt{q^2}\,\mathcal{B}_{T,0} &= (m_B^2+q^2)\,\mathcal{B}_{V,0} + (m_B^2-q^2)\,\mathcal{B}_{V,t}\,,\\ 2m_B\sqrt{q^2}\,\mathcal{B}_{T,1} &= (m_B^2+q^2)\,\mathcal{B}_{V,1} + (m_B^2-q^2)\,\mathcal{B}_{V,2}\,,\\ 2m_B\sqrt{q^2}\,\mathcal{B}_{T,2} &= (m_B^2+q^2)\,\mathcal{B}_{V,2} + (m_B^2-q^2)\,\mathcal{B}_{V,1}\,.\end{aligned} \quad (68)$$

Furthermore, in the limit of large recoil energy to the final state meson, one obtains additional relations [41, 42] that follow from the factorisation of soft and collinear QCD

dynamics [43–45]. Excluding radiative corrections for $q^2, m_L^2 \ll m_B^2$, and using the FFs $\mathcal{A}$ and $\mathcal{B}$, these relations read:

$$\mathcal{A}_{V,0} \simeq \mathcal{A}_{V,t} \simeq \frac{m_B}{\sqrt{q^2}}\,\mathcal{A}_{T,0}\,, \tag{69}$$

and

$$\mathcal{B}_{V,0} \simeq \mathcal{B}_{V,t} \simeq \frac{m_B}{\sqrt{q^2}}\,\mathcal{B}_{T,0}\,, \qquad \mathcal{B}_{V,1} \simeq \mathcal{B}_{V,2} \simeq \frac{\sqrt{q^2}}{m_B}\,\mathcal{B}_{T,1} \simeq \frac{\sqrt{q^2}}{m_B}\,\mathcal{B}_{T,2}\,. \tag{70}$$

It is also useful to write the differential decay rates for $B \to P\ell^+\ell^-$ and $B \to V\ell^+\ell^-$ in the naive-factorization approximation in terms of the new FFs. For the decays into pseudoscalar mesons, we obtain the relatively simple expression

$$\begin{aligned}\frac{d\Gamma[B \to P\ell^+\ell^-]}{dq^2} &= 2\,\mathcal{N}^2\,\frac{\left(2m_b\,C_7^{\rm eff}\right)^2}{q^2}\,(\mathcal{A}_{T,0})^2 + 4\,\mathcal{N}^2\,\frac{\mathrm{Re}\left[2m_b\,C_7^{\rm eff}C_9^{\rm eff\,*}\right]}{\sqrt{q^2}}\,\mathcal{A}_{T,0}\,\mathcal{A}_{V,0} \\ &\quad + 2\,\mathcal{N}^2\left(|C_9^{\rm eff}|^2 + |C_{10}|^2\right)\,(\mathcal{A}_{V,0})^2\,,\end{aligned} \tag{71}$$

where the overall normalization is given by

$$\mathcal{N} = |V_{tb}\,V_{ts}^*|\left[\frac{G_F^2\alpha^2}{3\cdot 2^{10}\pi^5 m_B^3}\lambda^{3/2}\right]^{1/2}\,.$$

For decays into vector mesons, we decompose the doubly differential decay width as [22,46]

$$\frac{d^2\Gamma[B \to V\ell^+\ell^-]}{dq^2\,d\cos\theta} = \frac{3}{8}\left[(1+\cos^2\theta)\,H_T(q^2) + 2\cos\theta\,H_A(q^2) + 2\,(1-\cos^2\theta)\,H_L(q^2)\right]\,. \tag{72}$$

Here θ is the angle between the positively charged lepton and the 3-momentum of the $\bar{B}^0$ or B^-–meson, and the functions H_T, H_L, H_T are related to the transverse rate, the longitudinal rate and the forward-backward asymmetry, respectively. In terms of the new FFs, the naive-factorization approximation for the SM contribution results in

$$\begin{aligned}H_T(q^2) &= 2\,\mathcal{N}^2\,\frac{\left(2m_b\,C_7^{\rm eff}\right)^2}{q^2}\left((\mathcal{B}_{T,1})^2 + (\mathcal{B}_{T,2})^2\right) \\ &\quad + 4\,\mathcal{N}^2\,\frac{\mathrm{Re}\left[2m_b\,C_7^{\rm eff}C_9^{\rm eff\,*}\right]}{\sqrt{q^2}}\,(\mathcal{B}_{T,1}\,\mathcal{B}_{V,1} + \mathcal{B}_{T,2}\,\mathcal{B}_{V,2}) \\ &\quad + 2\,\mathcal{N}^2\left(|C_9^{\rm eff}|^2 + |C_{10}|^2\right)\left((\mathcal{B}_{V,1})^2 + (\mathcal{B}_{V,2})^2\right)\,,\end{aligned} \tag{73}$$

$$\begin{aligned}H_L(q^2) &= 2\,\mathcal{N}^2\,\frac{\left(2m_b\,C_7^{\rm eff}\right)^2}{q^2}\,(\mathcal{B}_{T,0})^2 + 4\,\mathcal{N}^2\,\frac{\mathrm{Re}\left[2m_b\,C_7^{\rm eff}C_9^{\rm eff\,*}\right]}{\sqrt{q^2}}\,\mathcal{B}_{T,0}\,\mathcal{B}_{V,0} \\ &\quad + 2\,\mathcal{N}^2\left(|C_9^{\rm eff}|^2 + |C_{10}|^2\right)\,(\mathcal{B}_{V,0})^2\,,\end{aligned} \tag{74}$$

$$H_A(q^2) = 8\,\mathcal{N}^2\,\mathrm{Re}\left\{C_9^{\rm eff\,*}\,C_{10}\,\mathcal{B}_{V,1}\,\mathcal{B}_{V,2} + \frac{m_b}{\sqrt{q^2}}\,C_7^{\rm eff}\,C_{10}\,(\mathcal{B}_{T,1}\,\mathcal{B}_{V,2} + \mathcal{B}_{T,2}\,\mathcal{B}_{V,1})\right\}\,. \tag{75}$$

Finally, we note the simple FF dependence of the differential decay width and the longitudinal polarization fraction F_L of the vector meson in the decays $B \to V\nu\bar{\nu}$. In the absence of right-handed currents, we obtain [47]

$$\frac{d\Gamma[B \to V\nu\bar{\nu}]}{dq^2} = 12\,\mathcal{N}^2\,C_L^{\nu}\left((\mathcal{B}_{V,0})^2 + (\mathcal{B}_{V,1})^2 + (\mathcal{B}_{V,2})^2\right)\,, \tag{76}$$

and

$$F_L(q^2) = \frac{(\mathcal{B}_{V,0})^2}{(\mathcal{B}_{V,0})^2 + (\mathcal{B}_{V,1})^2 + (\mathcal{B}_{V,2})^2}\,. \tag{77}$$

At the kinematic endpoint $\mathcal{B}_{V,1}(t_-)$ vanishes, and (66) implies $F_L(t_-) = 1/3$, as required on general grounds.

C Calculation of Wilson Coefficients χ_I^X

C.1 Perturbative Contribution

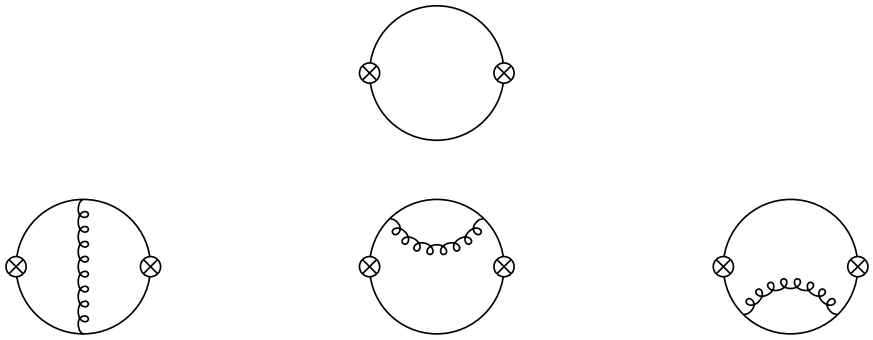

Figure 14: One- and two-loop diagrams contributing to the correlation function. The crossed circle indicates the insertion of the corresponding scalar, vector or tensor currents. The counter-term diagrams related to the fermion self-energies are not shown.

In this section, we will briefly sketch the evaluation of the one- and two-loop diagrams (see Fig. 14) contributing to the perturbative part of the correlation functions. We will specify the necessary number n of subtractions for the scalar, vector and tensor correlators, and determine the corresponding values of $\chi_I^X(n)$ from the Taylor expansion of the Wilson coefficients at $q^2 = 0$. This leads to a major simplification in the calculation, which allows to eliminate external momenta in propagator denominators and to use tensor reduction and recursion relations to express the two-loop integrals in terms of two fundamental master integrals. Furthermore, we will follow the procedure explained in [48] and absorb the IR-sensitive contributions to the Feynman integrals (in the limit $m \to 0$) into the corresponding condensate terms, such that our results have a finite limit when $m \to 0$.

We will find in useful to present the result in terms of the dimensionless variable

$$v \equiv \frac{M-m}{M+m}\,, \tag{78}$$

where M and m are the masses of the heavy and light quark in the loop. We further define the functions

$$\begin{aligned}
f_1(v) &\equiv \frac{1-v^2}{v}\,\mathrm{atanh}[v]\,,\\
f_2(v) &\equiv \frac{1}{v}\,\ln\left[\frac{1-v}{1+v}\right] - \frac{2}{1-v}\,\ln\left[\frac{1+v}{2}\right] - \frac{2}{1+v}\,\ln\left[\frac{1-v}{2}\right]\,,\\
f_3(v) &\equiv \frac{1}{v}\,\mathrm{Li}_2\left[\frac{4v}{(1+v)^2}\right] - \frac{1}{v}\,\mathrm{Li}_2\left[-\frac{4v}{(1-v)^2}\right] - \frac{4\,(1+v^2)}{v^2}\,\mathrm{atanh}^2[v]\,,
\end{aligned} \tag{79}$$

which are manifestly symmetric under exchange of light and heavy quarks ($v \to -v$), and take finite values in the limits $v \to \{-1, 0, 1\}$.

We will quote our results for scalar, vector and tensor currents. The expressions for currents with opposite parity can be simply obtained by changing $v \to 1/v$. Our expressions for scalar and vector currents coincide with [48]; the results for the tensor currents are new.

Scalar Correlator: For the correlator of two scalar currents, we obtain

$$\chi^S(n=2)\Big|_{\rm LO} = \frac{(3+v^2)(3v^2-1)}{64\pi^2(M+m)^2\,v^4} \overset{v\to 1}{\to} \frac{1}{8\pi^2 M^2}\,, \tag{80}$$

$$\begin{aligned}
\chi^S(n=2)\Big|_{\rm NLO} &= \frac{\alpha_s C_F}{4\pi}\,\frac{1}{64\pi^2(M+m)^2\,v^4}\Bigg\{\\
&\quad 6\left(3f_1\,(1-v^2)^2 + (3+v^2)(3v^2-1)\right)\left(f_2\,(1-v^2) - 4\,\ln\left[\frac{m+M}{\mu}\right]\right)\\
&\quad -f_1^2\left(11v^4-50v^2+23\right) + f_1\left(47v^4-126v^2+103\right)\\
&\quad +4\,f_3\,v^2\,(5v^2-1) + 2\left(29v^4+65v^2-40\right)\Bigg\}\\
&\overset{v\to 1}{\to} \frac{1}{8\pi^2 M^2}\,\frac{\alpha_s C_F}{4\pi}\left\{-24\,\ln\left[\frac{M}{\mu}\right] + \frac{2\pi^2}{3} + \frac{27}{2}\right\}.
\end{aligned} \tag{81}$$

Vector Correlator: For the different projections of the correlator of two vector currents, we obtain

$$\chi_L^V(n=1)\Big|_{\rm LO} = \frac{(3+v^2)(3v^2-1)}{64\pi^2\,v^2} \overset{v\to 1}{\to} \frac{1}{8\pi^2}\,, \tag{82}$$

$$\chi_L^V(n=1)\Big|_{\rm NLO} = \frac{\alpha_s C_F}{4\pi}\,\frac{1}{64\pi^2\,v^2}\Bigg\{$$

$$
\begin{aligned}
& f_1^2\left(25v^4+14v^2-23\right)+2f_1\left(19v^4-6v^2+23\right) \\
& +4f_3\,v^2\left(5v^2-1\right)-23+14v^2+13v^4\Bigg\}, \\
\overset{v\to 1}{\to}\quad & \frac{\alpha_s C_F}{4\pi}\,\frac{1}{8\pi^2}\left(\frac{1}{2}+\frac{2\pi^2}{3}\right), \qquad (83)
\end{aligned}
$$

and

$$
\chi_T^V(n=2)\Big|_{\rm LO} = \frac{-21v^6+53v^4+13v^2+3}{512\pi^2\,(M+m)^2\,v^4} \overset{v\to 1}{\to} \frac{3}{32\pi^2M^2}, \qquad (84)
$$

$$
\begin{aligned}
\chi_T^V(n=2)\Big|_{\rm NLO} = & \frac{\alpha_s C_F}{4\pi}\,\frac{1}{1536\pi^2\,(M+m)^2\,v^4}\Bigg\{ \\
& -f_1^2\left(803v^6-863v^4-155v^2-73\right)-2f_1\left(677v^6-741v^4+279v^2+73\right) \\
& -4f_3\,v^2\left(19v^4-86v^2-5\right)+73+323v^2+755v^4-551v^6\Bigg\}, \\
\overset{v\to 1}{\to}\quad & \frac{\alpha_s C_F}{4\pi}\,\frac{3}{32\pi^2M^2}\left(\frac{25}{6}+\frac{2\pi^2}{3}\right). \qquad (85)
\end{aligned}
$$

Tensor Correlator: The relevant projection of the tensor current gives rise to

$$
\begin{aligned}
\chi_T^T(n=3)\big|_{LO} = & \frac{-9f_1\left(v^2-1\right)^2\left(3v^2+1\right)+4\left(-9v^6+21v^4+v^2+3\right)}{256\pi^2\left(m+M\right)^2v^4} \\
\overset{v\to 1}{\to}\quad & \frac{1}{4\pi^2M^2} \qquad (86)
\end{aligned}
$$

$$
\begin{aligned}
\chi_T^T(n=3)\big|_{NLO} = & \frac{\alpha_s C_F}{4\pi}\,\frac{1}{384\pi^2(M+m)^2v^4}\Bigg\{ \\
& 12\left(3(v^2-1)^2(3v^2+1)f_1-3-v^2-21v^4+9v^6\right) \\
& \quad\times\left(f_2\left(1-v^2\right)-4\,\ln\left[\frac{m+M}{\mu}\right]\right) \\
& -f_1^2\left(766v^6-598v^4-142v^2-218\right) \\
& -f_1\left(1091v^6-1137v^4+297v^2+325\right) \\
& -8f_3\,v^2\left(7v^4-26v^2-5\right)+107+69v^2+469v^4-325v^6\Bigg\} \\
\overset{v\to 1}{\to}\quad & \frac{\alpha_s C_F}{4\pi}\,\frac{1}{4\pi^2M^2}\left(\frac{10}{3}+\frac{2\pi^2}{3}+8\ln\left[\frac{M}{\mu}\right]\right). \qquad (87)
\end{aligned}
$$

C.2 Condensate Contribution to the Correlation Functions

In this section we provide the expressions for the contributions of the gluon condensate, the quark condensate and the mixed quark-gluon condensate to the various current correlators.

The contributions to the coefficient of the scalar and vector correlators to all orders in the quark mass and lowest order in the coupling constant can already be found in [48], and we reproduce the results given in that paper. We extend this analysis by determining the coefficient functions for the tensor correlators. For the quark and the quark-gluon condensate, we employ techniques analogous to that given in [48] and closely follow their notation. In case of the gluon condensate, we use the plane-wave technique.

Quark Condensate and Quark–Gluon Condensate: The starting point for calculating the coefficient functions to all orders in the quark masses is a closed expression for the non-local quark condensate. The position-space expressions for the projection of the non-local quark condensates on the local quark condensate $\left\langle :\bar{q}q: \right\rangle^{(0)}$ and the local mixed quark-gluon condensate $\left\langle :g_s\bar{q}\sigma Fq: \right\rangle^{(0)}$ read

$$\begin{aligned}
\left\langle :\bar{q}_\alpha(0)q_\beta(x): \right\rangle_{\bar{q}q} &= \frac{1}{4m}\left\langle :\bar{q}q: \right\rangle^{(0)}\Gamma\left(\frac{D}{2}\right)(i\not{\partial}+m)_{\beta\alpha}\sum_{n=0}^{\infty}\frac{(-m^2x^2/4)^n}{n!\,\Gamma(n+D/2)}\,, \\
\left\langle :\bar{q}_\alpha(0)q_\beta(x): \right\rangle_{\bar{q}Fq} &= -\frac{1}{8m^3}\left\langle :g_s\bar{q}\sigma Fq: \right\rangle^{(0)}\Gamma\left(\frac{D}{2}\right) \\
&\quad\times\sum_{n=0}^{\infty}\Big[\,(n-1)i\not{\partial}+n\,m\,\Big]_{\beta\alpha}\frac{(-m^2x^2/4)^n}{n!\,\Gamma(n+D/2)}\,. \qquad (88)
\end{aligned}$$

Here α and β indicate the spinor indices. The corresponding projection of the non-local mixed quark-gluon condensate reads

$$\begin{aligned}
\left\langle :g_s\bar{q}_\alpha(0)F_{\mu\nu}(0)\,q_\beta(x): \right\rangle_{\bar{q}Fq} &= \frac{1}{4(D-1)(D-2)\,m^2}\left\langle :g_s\bar{q}\sigma Fq: \right\rangle^{(0)}\Gamma\left(\frac{D}{2}\right) \\
&\quad\times\Big[\Big(\big(\gamma_\mu\partial_\nu-\gamma_\nu\partial_\mu\big)+m\sigma_{\mu\nu}\Big)\big(i\not{\partial}+m\big)\Big]_{\beta\alpha}\sum_{n=0}^{\infty}\frac{(-m^2x^2/4)^n}{n!\Gamma(n+D/2)}\,. \qquad (89)
\end{aligned}$$

The relevant diagrams for the contribution of the non-local quark condensate and the non-local mixed quark-gluon condensate are given in Figs. 15 and C.2, respectively. The

Figure 15: Diagrams involving the non-local quark condensate, indicated by the two solid dots. The crossed circle symbolises the insertion of the currents.

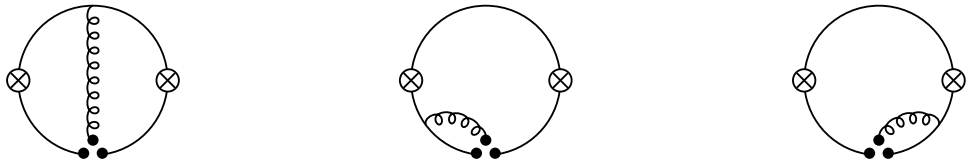

Figure 16: Diagrams involving the non-local mixed quark-gluon condensate, indicated by the three solid dots.

evaluation of the diagrams is simplified by the use of the equations of motion,

$$\left(\not{p} - m\right) \left\langle : g_s \bar{q}_\alpha(0) F_{\mu\nu}(0) q_\beta(x) : \right\rangle_{\bar{q}Fq} = 0\,, \tag{90}$$

$$\left(p^2 - m^2\right) \left\langle : \bar{q}(0)\tilde{q}(p) : \right\rangle_{\bar{q}Fq} = -\frac{\left\langle : g_s \bar{q}\sigma F q : \right\rangle^{(0)}}{2\left\langle : \bar{q}q : \right\rangle^{(0)}} \left\langle : \bar{q}(0)\tilde{q}(p) : \right\rangle_{\bar{q}q}\,, \tag{91}$$

$$\left(\not{p} - m\right) \left\langle : \bar{q}(0)\tilde{q}(p) : \right\rangle_{\bar{q}q} = 0\,. \tag{92}$$

Gluon Condensate: For the gluon condensate, it is more convenient to use the so-called fixed-point gauge technique, which is described in detail in [49]. In the framework of the fixed-point gauge, it is possible to derive an expression for

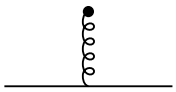

$$= -\frac{i}{4} g t^a G^a_{\kappa\lambda}(0) \frac{1}{(p^2 - m^2)} \left\{ \sigma_{\kappa\lambda}(\not{p} + m) + (\not{p} + m)\sigma_{\kappa\lambda} \right\}\,, \tag{93}$$

which is the basic building block for three lowest-order diagrams shown in Fig. 17.

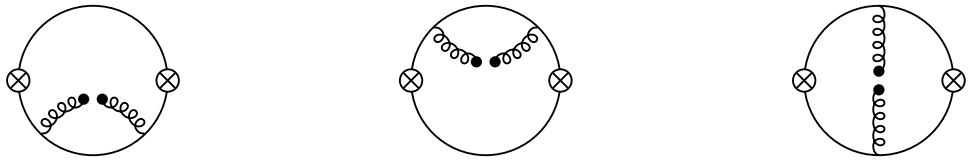

Figure 17: Diagrams involving the gluon condensate.

C.2.1 Results

Quark Condensate: The quark-condensate contribution to the coefficient for the scalar correlation function is given by

$$\chi^S(n=2)\Big|_{\bar{q}q} \;=\; \frac{\langle\bar{q}q\rangle\,(v+1)^3}{8(m+M)^5v^5} \;\stackrel{v\to 1}{\to}\; \frac{\langle\bar{q}q\rangle}{M^5}\,. \tag{94}$$

The same expression (up to an overall normalization factor) is obtained in case of the longitudinal projection of the vector correlator, $\chi_L^V(n=1)\big|_{\bar{q}q} = (M+m)^2v^2\,\chi^S(n=2)\big|_{\bar{q}q}$. The transverse projection of the vector correlator leads to

$$\chi_T^V(n=2)\Big|_{\bar{q}q} \;=\; -\frac{\langle\bar{q}q\rangle\,(v+1)^3}{64(m+M)^5v^5}\left(7v^2+1\right) \;\stackrel{v\to 1}{\to}\; -\frac{\langle\bar{q}q\rangle}{M^5}\,. \tag{95}$$

Finally, from the relevant tensor correlator we obtain

$$\chi_T^T(n=3)\Big|_{\bar{q}q} \;=\; -\frac{\langle\bar{q}q\rangle\,(v+1)^3}{32(m+M)^5v^5}\left(3v^2+1\right) \;\stackrel{v\to 1}{\to}\; -\frac{\langle\bar{q}q\rangle}{M^5}\,. \tag{96}$$

Gluon Condensate: The expressions for the gluon-condensate contributions to the various χ_I^X coefficients read as follows: For the scalar correlator we obtain

$$\begin{aligned}\chi^S(n=2)\Big|_{G^2} \;=\;& \frac{\left\langle\frac{\alpha}{\pi}G^2\right\rangle}{96\,(m+M)^6\,v^6}\Bigg\{15f_1\,(1-v^2)^2-15-4v^2+27v^4\\ &-6v^2(1-v^2)\left(f_2\,(1-v^2)-4\,\ln\left[\frac{m+M}{\mu}\right]\right)\Bigg\}\\ \stackrel{v\to 1}{\to}\;& \frac{\left\langle\frac{\alpha}{\pi}G^2\right\rangle}{12M^6}\,.\end{aligned} \tag{97}$$

Again, the same expression is obtained for the longitudinal projection of the vector correlator, $\chi_L^V(n=1)\big|_{GG} = (M+m)^2v^2\,\chi^S(n=2)\big|_{GG}$. For the transverse projection of the vector correlator, one has

$$\begin{aligned}\chi_T^V(n=2)\Big|_{G^2} \;=\;& \frac{\left\langle\frac{\alpha}{\pi}G^2\right\rangle}{384\,(m+M)^6\,v^6}\Bigg\{\\ &45+115v^2+3v^4-195v^6-5f_1\,(1-v^2)^2\left(25v^2+9\right)\\ &+v^2(1-v^2)\left(35v^2+41\right)\left(f_2\,(1-v^2)-4\,\ln\left[\frac{m+M}{\mu}\right]\right)\Bigg\}\\ \stackrel{v\to 1}{\to}\;& -\frac{\left\langle\frac{\alpha}{\pi}G^2\right\rangle}{12M^6}\,,\end{aligned} \tag{98}$$

and for the tensor correlator, we get

$$\chi_T^T(n=3)\Big|_{G^2} \;=\; \frac{\left\langle\frac{\alpha}{\pi}G^2\right\rangle}{384\,(m+M)^6\,v^6}\Bigg\{$$

$$
\begin{aligned}
& 105 + 91v^2 - 17v^4 - 195v^6 - 5f_1\,(1-v^2)^2\left(27v^2+17\right) \\
& +2(1-v^2)\left(15v^4+24v^2+5\right)\left(f_2\,(1-v^2) - 4\,\ln\left[\frac{m+M}{\mu}\right]\right)\Bigg\} \\
\stackrel{v\to 1}{\to}\;\; & -\frac{\left\langle \frac{\alpha}{\pi} G^2\right\rangle}{24M^6}\,. \qquad (99)
\end{aligned}
$$

Mixed Condensate: For the mixed-condensate contributions, we finally obtain

$$
\chi^S(n=2)\big|_{\bar{q}Gq} \;=\; -\frac{\left\langle\bar{q}Gq\right\rangle(1+v)}{4(m+M)^7v^5}\,(2+v) \;\stackrel{v\to 1}{\to}\; -\frac{3\left\langle\bar{q}Gq\right\rangle}{2M^7}\,, \qquad (100)
$$

and

$$
\chi_L^V(n=1)\big|_{\bar{q}Gq} \;=\; -\frac{\left\langle\bar{q}Gq\right\rangle(1+v)}{4(m+M)^5v^3}\,(2+v) \;\stackrel{v\to 1}{\to}\; -\frac{3\left\langle\bar{q}Gq\right\rangle}{2M^5}\,, \qquad (101)
$$

where $\chi_L^V(n=1)\big|_{\bar{q}Gq}$ is again proportional to $\chi^S(n=2)\big|_{\bar{q}Gq}$, as well as

$$
\chi_T^V(n=2)\big|_{\bar{q}Gq} \;=\; \frac{\left\langle\bar{q}Gq\right\rangle(1+v)}{96(m+M)^7v^5}\left(35v^3+59v^2+41v+9\right) \;\stackrel{v\to 1}{\to}\; \frac{3\left\langle\bar{q}Gq\right\rangle}{M^7}\,, \qquad (102)
$$

and

$$
\begin{aligned}
\chi^{TT}(n=3)\big|_{\bar{q}Gq} \;&=\; \frac{\left\langle\bar{q}Gq\right\rangle(1+v)}{48(m+M)^7v^6}\left(15v^4+28v^3+24v^2+12v+5\right) \\
&\stackrel{v\to 1}{\to}\; \frac{7\left\langle\bar{q}Gq\right\rangle}{2M^7}\,. \qquad (103)
\end{aligned}
$$

D Decomposition of the tensor-current correlator

Using the projectors

$$
P_L^{\mu\nu} = \frac{q^\mu q^\nu}{q^2}\,, \qquad P_T^{\mu\nu} = \frac{(q^\mu q^\nu - g^{\mu\nu}q^2)}{(D-1)q^2}\,, \qquad (104)
$$

we decompose the correlator of general tensor currents,

$$
\Pi_{\mu\nu\alpha\beta} \;=\; i\int d^4x\, e^{iqx}\,\langle 0|T[\bar{q}_1(x)\sigma_{\mu\nu}q_2(x)\;\bar{q}_2(0)\sigma_{\alpha\beta}q_1(0)]|0\rangle\,, \qquad (105)
$$

into the two Lorentz-invariant functions Π_{TT} and Π_{LT} as follows,

$$
\begin{aligned}
\Pi_{\mu\nu\alpha\beta} \;&=\; [g_{\mu\alpha}g_{\nu\beta} - g_{\mu\beta}g_{\nu\alpha}]\frac{3\Pi_{TT}(q^2)}{2} \\
&+ \frac{g_{\mu\beta}q_\nu q_\alpha + g_{\nu\alpha}q_\mu q_\beta - g_{\mu\alpha}q_\nu q_\beta - g_{\nu\beta}q_\mu q_\alpha}{q^2}\left(\frac{3\Pi_{TT}(q^2)}{2} + \Pi_{LT}(q^2)\right)\,, \qquad (106)
\end{aligned}
$$

where

$$\begin{aligned} P_L^{\mu\alpha}\, P_T^{\nu\beta}\, \Pi_{\mu\nu\alpha\beta} &= P_T^{\mu\alpha}\, P_L^{\nu\beta}\, \Pi_{\mu\nu\alpha\beta} = \Pi_{LT}(q^2)\,, \\ P_T^{\mu\alpha}\, P_T^{\nu\beta}\, \Pi_{\mu\nu\alpha\beta} &= \Pi_{TT}(q^2)\,, \\ P_L^{\mu\alpha}\, P_L^{\nu\beta}\, \Pi_{\mu\nu\alpha\beta} &= 0\,. \end{aligned} \tag{107}$$

In this notation, the correlator of the currents

$$j_\mu^T = \bar{q}\sigma_{\mu\alpha}q^\alpha q \tag{108}$$

leads to $q^2\,\Pi_{LT}(q^2)$.

E Covariance Matrices

Here we give the covariance matrices as defined in (58) for the parameters corresponding to the best-fit parameters in Tables 5 to 12.

$B \to K$ form factor fit:

- The fit of $B \to K$ FFs to LCSR data alone gives the covariances matrices:

	SE	SSE
$\mathcal{A}_{V,0}$	$\begin{pmatrix} 1.56\times10^{-5} & -1.04\times10^{-4} \\ -1.04\times10^{-4} & 9.59\times10^{-4} \end{pmatrix}$	$\begin{pmatrix} 4.39\times10^{-3} & -2.91\times10^{-2} \\ -2.91\times10^{-2} & 0.266 \end{pmatrix}$
$\mathcal{A}_{V,t}^{\text{no res.}}$	$\begin{pmatrix} 1.19\times10^{-4} & -7.87\times10^{-4} \\ -7.87\times10^{-4} & 6.98\times10^{-3} \end{pmatrix}$	$\begin{pmatrix} 7.17\times10^{-3} & -4.75\times10^{-2} \\ -4.75\times10^{-2} & 0.423 \end{pmatrix}$
$\mathcal{A}_{V,t}$	$\begin{pmatrix} 6.27\times10^{-6} & -2.72\times10^{-5} \\ -2.72\times10^{-5} & 2.19\times10^{-4} \end{pmatrix}$	$\begin{pmatrix} 2.61\times10^{-3} & -1.08\times10^{-2} \\ -1.08\times10^{-2} & 8.86\times10^{-2} \end{pmatrix}$
$\mathcal{A}_{T,0}$	$\begin{pmatrix} 2.1\times10^{-5} & -6.55\times10^{-5} \\ -6.55\times10^{-5} & 5.37\times10^{-4} \end{pmatrix}$	$\begin{pmatrix} 7.63\times10^{-4} & 6.3\times10^{-4} \\ 6.3\times10^{-4} & 8.32\times10^{-3} \end{pmatrix}$

- For the fit of scalar/vector $B \to K$ FFs to LCSR and Lattice data, we obtain the covariance matrices:

	SE	SSE
$\mathcal{A}_{V,0}$	$\begin{pmatrix} 1.48\times10^{-5} & -9.81\times10^{-5} \\ -9.81\times10^{-5} & 8.76\times10^{-4} \end{pmatrix}$	$\begin{pmatrix} 6.26\times10^{-3} & -4.15\times10^{-2} \\ -4.15\times10^{-2} & 0.382 \end{pmatrix}$
$\mathcal{A}_{V,t}^{\text{no res.}}$	$\begin{pmatrix} 4.82\times10^{-5} & -2.03\times10^{-4} \\ -2.03\times10^{-4} & 1.6\times10^{-3} \end{pmatrix}$	$\begin{pmatrix} 3.08\times10^{-3} & -1.39\times10^{-2} \\ -1.39\times10^{-2} & 0.11 \end{pmatrix}$
$\mathcal{A}_{V,t}$	$\begin{pmatrix} 6.21\times10^{-5} & -4.11\times10^{-4} \\ -4.11\times10^{-4} & 3.75\times10^{-3} \end{pmatrix}$	$\begin{pmatrix} 3.45\times10^{-3} & -2.37\times10^{-2} \\ -2.37\times10^{-2} & 0.261 \end{pmatrix}$

$B \to \rho$ form factor fit:

- Fitting to LCSR data alone, the covariance matrices for the $B \to \rho$ FFs are given by:

	SE	SSE
$\mathcal{B}_{V,0}$	$\begin{pmatrix} 4.15 \times 10^{-6} & -3.2 \times 10^{-5} \\ -3.2 \times 10^{-5} & 7.93 \times 10^{-4} \end{pmatrix}$	$\begin{pmatrix} 5.26 \times 10^{-3} & -4.33 \times 10^{-2} \\ -4.33 \times 10^{-2} & 1.57 \end{pmatrix}$
$\mathcal{B}_{V,1}$	$\begin{pmatrix} 1.57 \times 10^{-5} & -1.28 \times 10^{-4} \\ -1.28 \times 10^{-4} & 1.92 \times 10^{-3} \end{pmatrix}$	$\begin{pmatrix} 3.29 \times 10^{-3} & -2.7 \times 10^{-2} \\ -2.7 \times 10^{-2} & 0.396 \end{pmatrix}$
$\mathcal{B}_{V,2}$	$\begin{pmatrix} 6.45 \times 10^{-6} & -5.23 \times 10^{-5} \\ -5.23 \times 10^{-5} & 7.98 \times 10^{-4} \end{pmatrix}$	$\begin{pmatrix} 1.83 \times 10^{-3} & -1.42 \times 10^{-2} \\ -1.42 \times 10^{-2} & 0.274 \end{pmatrix}$
$\mathcal{B}_{V,t}$	$\begin{pmatrix} 1.19 \times 10^{-5} & -9.76 \times 10^{-5} \\ -9.76 \times 10^{-5} & 1.42 \times 10^{-3} \end{pmatrix}$	$\begin{pmatrix} 2.19 \times 10^{-3} & -1.81 \times 10^{-2} \\ -1.81 \times 10^{-2} & 0.258 \end{pmatrix}$
$\mathcal{B}_{T,0}$	$\begin{pmatrix} 1.01 \times 10^{-5} & 1.29 \times 10^{-4} \\ 1.29 \times 10^{-4} & 1.72 \times 10^{-2} \end{pmatrix}$	$\begin{pmatrix} 6.49 \times 10^{-3} & 9.63 \times 10^{-2} \\ 9.63 \times 10^{-2} & 15.3 \end{pmatrix}$
$\mathcal{B}_{T,1}$	$\begin{pmatrix} 7.45 \times 10^{-7} & -4.16 \times 10^{-6} \\ -4.16 \times 10^{-6} & 5.21 \times 10^{-5} \end{pmatrix}$	$\begin{pmatrix} 1.86 \times 10^{-3} & -9.82 \times 10^{-3} \\ -9.82 \times 10^{-3} & 0.13 \end{pmatrix}$
$\mathcal{B}_{T,2}$	$\begin{pmatrix} 2.7 \times 10^{-7} & -1.41 \times 10^{-6} \\ -1.41 \times 10^{-6} & 1.89 \times 10^{-5} \end{pmatrix}$	$\begin{pmatrix} 8.09 \times 10^{-4} & -2.15 \times 10^{-3} \\ -2.15 \times 10^{-3} & 6.88 \times 10^{-2} \end{pmatrix}$

- For the fit of vector and axial-vector $B \to \rho$ FFs to LCSR and Lattice data, the covariance matrices read:

	SE	SSE
$\mathcal{B}_{V,0}$	$\begin{pmatrix} 2.62 \times 10^{-6} & -1.35 \times 10^{-5} \\ -1.35 \times 10^{-5} & 5.35 \times 10^{-4} \end{pmatrix}$	$\begin{pmatrix} 2.86 \times 10^{-3} & -5.12 \times 10^{-3} \\ -5.12 \times 10^{-3} & 0.796 \end{pmatrix}$
$\mathcal{B}_{V,1}$	$\begin{pmatrix} 5.72 \times 10^{-6} & -3.08 \times 10^{-5} \\ -3.08 \times 10^{-5} & 9.15 \times 10^{-4} \end{pmatrix}$	$\begin{pmatrix} 1.24 \times 10^{-3} & -7.07 \times 10^{-3} \\ -7.07 \times 10^{-3} & 0.193 \end{pmatrix}$
$\mathcal{B}_{V,2}$	$\begin{pmatrix} 1.99 \times 10^{-6} & -3.02 \times 10^{-6} \\ -3.02 \times 10^{-6} & 2.26 \times 10^{-4} \end{pmatrix}$	$\begin{pmatrix} 5.21 \times 10^{-4} & 1.52 \times 10^{-3} \\ 1.52 \times 10^{-3} & 6.4 \times 10^{-2} \end{pmatrix}$

$B \to K^*$ form factor fit: The covariance matrices for the $B \to K^*$ FFs are given by:

	SE	SSE
$\mathcal{B}_{V,0}$	$\begin{pmatrix} 4.38\times10^{-6} & -3.12\times10^{-5} \\ -3.12\times10^{-5} & 1.08\times10^{-3} \end{pmatrix}$	$\begin{pmatrix} 4.85\times10^{-3} & -3.26\times10^{-2} \\ -3.26\times10^{-2} & 1.85 \end{pmatrix}$
$\mathcal{B}_{V,1}$	$\begin{pmatrix} 1.94\times10^{-5} & -1.63\times10^{-4} \\ -1.63\times10^{-4} & 3.06\times10^{-3} \end{pmatrix}$	$\begin{pmatrix} 3.\times10^{-3} & -2.54\times10^{-2} \\ -2.54\times10^{-2} & 0.467 \end{pmatrix}$
$\mathcal{B}_{V,2}$	$\begin{pmatrix} 1.01\times10^{-5} & -8.52\times10^{-5} \\ -8.52\times10^{-5} & 1.59\times10^{-3} \end{pmatrix}$	$\begin{pmatrix} 2.42\times10^{-3} & -1.87\times10^{-2} \\ -1.87\times10^{-2} & 0.456 \end{pmatrix}$
$\mathcal{B}_{V,t}$	$\begin{pmatrix} 1.79\times10^{-5} & -1.53\times10^{-4} \\ -1.53\times10^{-4} & 2.75\times10^{-3} \end{pmatrix}$	$\begin{pmatrix} 2.24\times10^{-3} & -1.93\times10^{-2} \\ -1.93\times10^{-2} & 0.34 \end{pmatrix}$
$\mathcal{B}_{T,0}$	$\begin{pmatrix} 1.63\times10^{-5} & 3.6\times10^{-4} \\ 3.6\times10^{-4} & 2.41\times10^{-2} \end{pmatrix}$	$\begin{pmatrix} 9.38\times10^{-3} & 0.246 \\ 0.246 & 17.7 \end{pmatrix}$
$\mathcal{B}_{T,1}$	$\begin{pmatrix} 1.17\times10^{-6} & -6.23\times10^{-6} \\ -6.23\times10^{-6} & 9.82\times10^{-5} \end{pmatrix}$	$\begin{pmatrix} 2.26\times10^{-3} & -1.12\times10^{-2} \\ -1.12\times10^{-2} & 0.191 \end{pmatrix}$
$\mathcal{B}_{T,2}$	$\begin{pmatrix} 4.04\times10^{-7} & -2.07\times10^{-6} \\ -2.07\times10^{-6} & 3.4\times10^{-5} \end{pmatrix}$	$\begin{pmatrix} 1.12\times10^{-3} & -2.27\times10^{-3} \\ -2.27\times10^{-3} & 0.11 \end{pmatrix}$

$B_s \to \phi$ form factor fit: The covariance matrices for the $B_s \to \phi$ FFs are given by:

	SE	SSE
$\mathcal{B}_{V,0}$	$\begin{pmatrix} 1.16\times10^{-6} & -8.32\times10^{-6} \\ -8.32\times10^{-6} & 3.47\times10^{-4} \end{pmatrix}$	$\begin{pmatrix} 4.56\times10^{-3} & -2.81\times10^{-2} \\ -2.81\times10^{-2} & 1.98 \end{pmatrix}$
$\mathcal{B}_{V,1}$	$\begin{pmatrix} 8.44\times10^{-6} & -7.79\times10^{-5} \\ -7.79\times10^{-5} & 1.63\times10^{-3} \end{pmatrix}$	$\begin{pmatrix} 3.37\times10^{-3} & -3.15\times10^{-2} \\ -3.15\times10^{-2} & 0.643 \end{pmatrix}$
$\mathcal{B}_{V,2}$	$\begin{pmatrix} 3.6\times10^{-6} & -3.26\times10^{-5} \\ -3.26\times10^{-5} & 7.08\times10^{-4} \end{pmatrix}$	$\begin{pmatrix} 2.91\times10^{-3} & -2.38\times10^{-2} \\ -2.38\times10^{-2} & 0.662 \end{pmatrix}$
$\mathcal{B}_{V,t}$	$\begin{pmatrix} 6.61\times10^{-6} & -6.07\times10^{-5} \\ -6.07\times10^{-5} & 1.28\times10^{-3} \end{pmatrix}$	$\begin{pmatrix} 2.05\times10^{-3} & -1.9\times10^{-2} \\ -1.9\times10^{-2} & 0.394 \end{pmatrix}$
$\mathcal{B}_{T,0}$	$\begin{pmatrix} 7.03\times10^{-6} & 1.75\times10^{-4} \\ 1.75\times10^{-4} & 1.04\times10^{-2} \end{pmatrix}$	$\begin{pmatrix} 1.41\times10^{-2} & 0.406 \\ 0.406 & 25.2 \end{pmatrix}$
$\mathcal{B}_{T,1}$	$\begin{pmatrix} 6.39\times10^{-7} & -3.91\times10^{-6} \\ -3.91\times10^{-6} & 6.67\times10^{-5} \end{pmatrix}$	$\begin{pmatrix} 3.37\times10^{-3} & -1.93\times10^{-2} \\ -1.93\times10^{-2} & 0.35 \end{pmatrix}$
$\mathcal{B}_{T,2}$	$\begin{pmatrix} 1.63\times10^{-7} & -8.97\times10^{-7} \\ -8.97\times10^{-7} & 1.69\times10^{-5} \end{pmatrix}$	$\begin{pmatrix} 1.64\times10^{-3} & -3.86\times10^{-3} \\ -3.86\times10^{-3} & 0.187 \end{pmatrix}$

References

[1] M. Artuso *et. al.*, *B, D and K decays*, *Eur. Phys. J.* **C57** (2008) 309–492, [arXiv:0801.1833].

[2] M. Antonelli *et. al.*, *Flavor Physics in the Quark Sector*, arXiv:0907.5386.

[3] J. A. Bailey *et. al.*, *The $B \to \pi \ell \nu$ semileptonic form factor from three-flavor lattice QCD: A Model-independent determination of $|V_{ub}|$*, *Phys. Rev.* **D79** (2009) 054507, [arXiv:0811.3640].

[4] **QCDSF** Collaboration, A. Al-Haydari *et. al.*, *Semileptonic form factors $D \to \pi, K$ and $B \to \pi, K$ from a fine lattice*, *Eur. Phys. J.* **A43** (2010) 107–120, [arXiv:0903.1664].

[5] C. Bernard *et. al.*, *Visualization of semileptonic form factors from lattice QCD*, *Phys. Rev.* **D80** (2009) 034026, [arXiv:0906.2498].

[6] E. Dalgic *et. al.*, *B Meson Semileptonic Form Factors from Unquenched Lattice QCD*, *Phys. Rev.* **D73** (2006) 074502, [hep-lat/0601021].

[7] **UKQCD** Collaboration, K. C. Bowler, J. F. Gill, C. M. Maynard, and J. M. Flynn, *$B \to \rho l \nu$ form factors in lattice QCD*, *JHEP* **05** (2004) 035, [hep-lat/0402023].

[8] P. Ball and R. Zwicky, *New results on $B \to \pi, K, \eta$ decay form factors from light-cone sum rules*, *Phys.Rev.* **D71** (2005) 014015, [hep-ph/0406232].

[9] P. Ball and R. Zwicky, *$B_{d,s} \to \rho, \omega, K^*, \phi$ Decay Form Factors from Light-Cone Sum Rules Revisited*, *Phys. Rev.* **D71** (2005) 014029, [hep-ph/0412079].

[10] P. Colangelo and A. Khodjamirian, *QCD sum rules, a modern perspective*, hep-ph/0010175.

[11] D. Becirevic and A. B. Kaidalov, *Comment on the heavy $\to$ light form factors*, *Phys. Lett.* **B478** (2000) 417–423, [hep-ph/9904490].

[12] J. M. Flynn and J. Nieves, *$|V_{ub}|$ from exclusive semileptonic $B \to \pi$ decays revisited*, *Phys. Rev.* **D76** (2007) 031302, [arXiv:0705.3553].

[13] C. Bourrely, I. Caprini, and L. Lellouch, *Model-independent description of $B \to \pi l \nu$ decays and a determination of $|V_{ub}|$*, *Phys. Rev.* **D79** (2009) 013008, [arXiv:0807.2722].

[14] M. C. Arnesen, B. Grinstein, I. Z. Rothstein, and I. W. Stewart, *A precision model independent determination of $|V_{ub}|$ from $B \to \pi e \nu$*, *Phys. Rev. Lett.* **95** (2005) 071802, [hep-ph/0504209].

[15] C. G. Boyd, B. Grinstein, and R. F. Lebed, *Constraints on form-factors for exclusive semileptonic heavy to light meson decays*, *Phys. Rev. Lett.* **74** (1995) 4603–4606, [hep-ph/9412324].

[16] C. G. Boyd and M. J. Savage, *Analyticity, shapes of semileptonic form factors, and $\bar{B} \to \pi \ell \bar{\nu}$*, *Phys. Rev.* **D56** (1997) 303–311, [hep-ph/9702300].

[17] I. Caprini, L. Lellouch, and M. Neubert, *Dispersive bounds on the shape of $\bar{B} \to D^{(*)} l \bar{\nu}$ form factors*, *Nucl. Phys.* **B530** (1998) 153–181, [hep-ph/9712417].

[18] T. Becher and R. J. Hill, *Comment on form factor shape and extraction of $|V_{ub}|$ from $B \to \pi \ell \nu$*, *Phys. Lett.* **B633** (2006) 61–69, [hep-ph/0509090].

[19] M. Beneke, T. Feldmann, and D. Seidel, *Exclusive radiative and electroweak $b \to d$ and $b \to s$ penguin decays at NLO*, *Eur. Phys. J.* **C41** (2005) 173–188, [hep-ph/0412400].

[20] C. Bobeth, G. Hiller, and G. Piranishvili, *Angular Distributions of $B \to K\, l\, l$ Decays*, *JHEP* **12** (2007) 040, [arXiv:0709.4174].

[21] U. Egede, T. Hurth, J. Matias, M. Ramon, and W. Reece, *New observables in the decay mode $\bar{B} \to \bar{K}^{*0} \ell^+ \ell^-$*, *JHEP* **11** (2008) 032, [arXiv:0807.2589].

[22] W. Altmannshofer *et. al.*, *Symmetries and Asymmetries of $B \to K^* \mu^+ \mu^-$. Decays in the Standard Model and Beyond*, *JHEP* **01** (2009) 019, [arXiv:0811.1214].

[23] M. Bartsch, M. Beylich, G. Buchalla, and D. N. Gao, *Precision Flavour Physics with $B \to K \nu \bar{\nu}$ and $B \to K \ell^+ \ell^-$*, *JHEP* **11** (2009) 011, [arXiv:0909.1512].

[24] P. Ball, *$|V_{ub}|$ from UTangles and $B \to \pi \ell \nu$*, *Phys. Lett.* **B644** (2007) 38–44, [hep-ph/0611108].

[25] **Particle Data Group**, C. Amsler *et. al.*, *Review of particle physics*, *Phys. Lett.* **B667** (2008) 1.

[26] W. A. Bardeen, E. J. Eichten, and C. T. Hill, *Chiral Multiplets of Heavy-Light Mesons*, *Phys. Rev.* **D68** (2003) 054024, [hep-ph/0305049].

[27] M. A. Shifman, A. I. Vainshtein, and V. I. Zakharov, *QCD and Resonance Physics. Sum Rules*, *Nucl. Phys.* **B147** (1979) 385–447.

[28] M. A. Shifman, A. I. Vainshtein, and V. I. Zakharov, *QCD and Resonance Physics: Applications*, *Nucl. Phys.* **B147** (1979) 448–518.

[29] V. A. Novikov, M. A. Shifman, A. I. Vainshtein, and V. I. Zakharov, *Operator expansion in quantum chromodynamics beyond perturbation theory*, *Nucl. Phys.* **B174** (1980) 378.

[30] R. J. Hill, *The modern description of semileptonic meson form factors*, hep-ph/0606023.

[31] C. Bernard *et. al.*, *Status of the MILC light pseudoscalar meson project*, *PoS* **LAT2007** (2007) 090, [arXiv:0710.1118].

[32] R. Williams, C. S. Fischer, and M. R. Pennington, *Extracting the $\bar{q}q$ condensate for light quarks beyond the chiral limit in models of QCD*, arXiv:0704.2296.

[33] M. V. Polyakov and C. Weiss, *Mixed quark-gluon condensate from instantons*, *Phys. Lett.* **B387** (1996) 841–847, [hep-ph/9607244].

[34] G. D'Agostini, *Asymmetric Uncertainties: Sources, Treatment and Potential Dangers*, physics/0403086.

[35] C. Bobeth, G. Hiller, and G. Piranishvili, *CP Asymmetries in bar $B \to \bar{K}^*(\to \bar{K}\pi)\bar{\ell}\ell$ and Untagged $\bar{B}_s$, $B_s \to \phi(\to K^+K^-)\bar{\ell}\ell$ Decays at NLO*, *JHEP* **07** (2008) 106, [arXiv:0805.2525].

[36] A. Bharucha and W. Reece, *Constraining new physics with $B \to K^*\mu^+\mu^-$ in the early LHC era*, arXiv:1002.4310.

[37] M. Beneke, T. Feldmann, and D. Seidel, *Systematic approach to exclusive $B \to V\ell^+\ell^-, V\gamma$ decays*, *Nucl. Phys.* **B612** (2001) 25–58, [hep-ph/0106067].

[38] B. Grinstein and D. Pirjol, *Precise $|V_{ub}|$ determination from exclusive B decays: Controlling the long-distance effects*, *Phys. Rev.* **D70** (2004) 114005, [hep-ph/0404250].

[39] S. Descotes-Genon and A. Le Yaouanc, *Parametrisations of the $D \to K\ell\nu$ form factor and the determination of $\hat{g}$*, *J. Phys.* **G35** (2008) 115005, [arXiv:0804.0203].

[40] **UKQCD** Collaboration, A. M. Green, J. Koponen, C. McNeile, C. Michael, and G. Thompson, *Excited B mesons from the lattice*, *Phys.Rev.* **D69** (2004) 094505, [hep-lat/0312007].

[41] J. Charles, A. Le Yaouanc, L. Oliver, O. Pene, and J. C. Raynal, *Heavy-to-light form factors in the heavy mass to large energy limit of QCD*, *Phys. Rev.* **D60** (1999) 014001, [hep-ph/9812358].

[42] M. Beneke and T. Feldmann, *Symmetry-breaking corrections to heavy-to-light B meson form factors at large recoil*, *Nucl. Phys.* **B592** (2001) 3–34, [hep-ph/0008255].

[43] M. Beneke and T. Feldmann, *Spectator interactions and factorization in $B \to \pi\ell\nu$ decay*, *Eur. Phys. J.* **C33** (2004) s241–s243, [hep-ph/0308303].

[44] B. O. Lange and M. Neubert, *Factorization and the soft overlap contribution to heavy- to-light form factors*, *Nucl. Phys.* **B690** (2004) 249–278, [hep-ph/0311345].

[45] M. Beneke and T. Feldmann, *Factorization of heavy-to-light form factors in soft-collinear effective theory*, *Nucl. Phys.* **B685** (2004) 249–296, [hep-ph/0311335].

[46] F. Krüger and J. Matias, *Probing new physics via the transverse amplitudes of $B^0 \to K^{*0}(\to K^-\pi^+)\ell^+\ell^-$ at large recoil*, *Phys. Rev.* **D71** (2005) 094009, [hep-ph/0502060].

[47] W. Altmannshofer, A. J. Buras, D. M. Straub, and M. Wick, *New strategies for New Physics search in $B \to K^*\nu\bar{\nu}$, $B \to K\nu\bar{\nu}$ and $B \to X_s\nu\bar{\nu}$ decays*, *JHEP* **04** (2009) 022, [arXiv:0902.0160].

[48] M. Jamin and M. Münz, *Current correlators to all orders in the quark masses*, *Z. Phys.* **C60** (1993) 569–578, [hep-ph/9208201].

[49] L. J. Reinders, H. Rubinstein, and S. Yazaki, *Hadron Properties from QCD Sum Rules*, *Phys. Rept.* **127** (1985) 1.